UC Irvine
UC Irvine Previously Published Works

Title

IL-10 Signaling Remodels Adipose Chromatin Architecture to Limit Thermogenesis and Energy Expenditure.

Permalink

Journal

ISSN

Authors

Rajbhandari, Prashant
Thomas, Brandon J
Feng, An-Chieh
et al.

Publication Date

DOI

Copyright Information

Peer reviewed

IL-10 Signaling Remodels Adipose Chromatin Architecture to Limit Thermogenesis and Energy Expenditure

Prashant Rajbhandari[1,9], **Brandon J. Thomas**[4,9], **An-Chieh Feng**[4], **Cynthia Hong**[1], **Jiexin Wang**[1], **Laurent Vergnes**[5], **Tamer Sallam**[6], **Bo Wang**[1], **Jaspreet Sandhu**[1], **Marcus M. Seldin**[4,5], **Aldons J. Lusis**[4,5], **Loren G. Fong**[6], **Melanie Katz**[7], **Richard Lee**[7], **Stephen G. Young**[6], **Karen Reue**[2,5], **Stephen T. Smale**[2,4,8], and **Peter Tontonoz**[1,2,3,8,10,*]

[1]Department of Pathology and Laboratory Medicine, David Geffen School of Medicine, University of California, Los Angeles, Los Angeles, CA 90095, USA

[2]Molecular Biology Institute, David Geffen School of Medicine, University of California, Los Angeles, Los Angeles, CA 90095, USA

[3]Howard Hughes Medical Institute, David Geffen School of Medicine, University of California, Los Angeles, Los Angeles, CA 90095, USA

[4]Department of Microbiology, Immunology, and Molecular Genetics, David Geffen School of Medicine, University of California, Los Angeles, Los Angeles, CA 90095, USA

[5]Department of Human Genetics, David Geffen School of Medicine, University of California, Los Angeles, Los Angeles, CA 90095, USA

[6]Department of Medicine, Division of Cardiology, David Geffen School of Medicine, University of California, Los Angeles, Los Angeles, CA 90095, USA

[7]Ionis Pharmaceuticals, Carlsbad, CA 92008, USA

SUMMARY

Signaling pathways that promote adipose tissue thermogenesis are well characterized, but the limiters of energy expenditure are largely unknown. Here, we show that ablation of the anti-inflammatory cytokine IL-10 improves insulin sensitivity, protects against diet-induced obesity, and elicits the browning of white adipose tissue. Mechanistic studies define bone marrow cells as the source of the IL-10 signal and adipocytes as the target cell type mediating these effects. IL-10 receptor alpha is highly enriched in mature adipocytes and is induced in response to differentiation, obesity, and aging. Assay for transposase-accessible chromatin sequencing (ATAC-

*Correspondence: ptontonoz@mednet.ucla.edu.
[8]Senior author
[9]These authors contributed equally
[10]Lead Contact

seq), ChIP-seq, and RNA-seq reveal that IL-10 represses the transcription of thermogenic genes in adipocytes by altering chromatin accessibility and inhibiting ATF and C/EBPβ recruitment to key enhancer regions. These findings expand our understanding of the relationship between inflammatory signaling pathways and adipose tissue function and provide insight into the physiological control of thermogenesis that could inform future therapy.

In Brief

An anti-inflammatory cytokine suppresses adipocyte thermogenesis to limit energy expenditure.
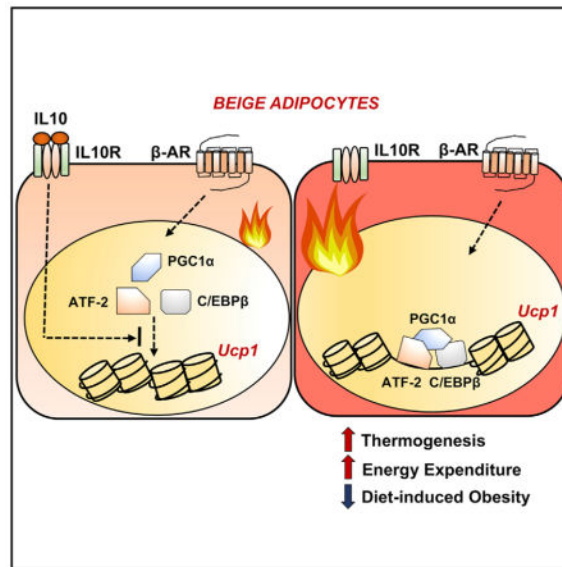
INTRODUCTION

White adipose tissue (WAT) stores energy in times of nutritional excess, and its dysfunction contributes to metabolic disorders such as type 2 diabetes (Rosen and Spiegelman, 2014). BAT is specialized to dissipate stored chemical energy in the form of heat, and BAT mass inversely correlates with body mass index and has been ascribed a potential anti-obesity function (van Marken Lichtenbelt et al., 2009; Virtanen et al., 2009). Recent studies have revealed the ability of certain WAT depots to activate thermogenesis upon exposure to cold and hormonal stimuli (Ohno et al., 2012; Tiraby and Langin, 2003). A subpopulation of cells in inguinal WAT (iWAT) known as "beige" cells expresses UCP1 and carries out thermogenesis (Wu et al., 2012). UCP1 is crucial for thermogenesis in both brown and beige adipocytes, and its activity contributes to regulation of energy balance (Feldmann et al., 2009).

Immune-adipose crosstalk has pronounced effects on the expansion and activation of beige adipose tissue. Several studies have highlighted the importance of anti-inflammatory (type II) cytokines in regulating adipose thermogenesis. Production of interleukin-4 (IL-4)/IL-13 by eosinophils upon stimulation by cold or exercise activates thermogenesis (Qiu et al., 2014; Rao et al., 2014). Activation of type 2 innate lymphoid (IL-C2) cells by IL-33 acts via IL-4Rα in pre-adipocytes to promote beige fat biogenesis (Lee et al., 2015). Recently, IL-33

was shown to license adipocytes for uncoupled respiration by regulating the splicing of UCP1 (Odegaard et al., 2016).

IL-10 is a type II cytokine with anti-inflammatory properties and its loss is associated with autoimmune pathologies (Couper et al., 2008). IL-10 is secreted by multiple immune cells, including macrophages, dendritic cells, B cells, and T cells (Saraiva and O'Garra, 2010). It signals through a receptor complex of IL-10Rα and IL-10Rβ to trigger the activation of signal transducer and activator of transcription 3 (STAT3) (Moore et al., 2001). STAT3 is essential for the anti-inflammatory activity of IL-10 (Lang et al., 2002), which are believed to be primarily due to repression of transcription. However, the precise mechanisms by which IL-10 regulates gene expression remain very poorly understood (Murray, 2005; Murray and Smale, 2012).

The role of IL-10 in adipose biology and energy homeostasis is largely unknown. Some studies have suggested that IL-10 might create an anti-inflammatory milieu by promoting the activity of M2 macrophages (Gao et al., 2013; Hong et al., 2009; Lumeng et al., 2007; Xie et al., 2014). However, loss-of-function studies have not supported an anti-obesity role for IL-10 (den Boer et al., 2006; Mauer et al., 2014; Miller et al., 2011). Furthermore, ablation of IL-10 does not cause insulin resistance (Kowalski et al., 2011). Here, we delineate a function for IL-10 signaling in directing transcriptional responses that limit thermogenesis. We show that bone-marrow-derived IL-10 acts on adipocytes via IL-10Rα to repress thermogenic gene expression by altering the chromatin landscape at transcriptional regulatory regions. These findings identify the IL-10 axis as a regulator of thermogenesis and expand our understanding of the links between immune signaling and adipose tissue function.

RESULTS

Ablation of IL-10 Protects Mice from Diet-Induced Obesity

To dissect the role of IL-10 in systemic metabolic homeostasis, we analyzed young *Il-10$^{-/-}$* mice (10 weeks of age) on a C57BL/6 background. IL-10 deficiency on this genetic background is associated with a relatively low incidence of colitis (Keubler et al., 2015). There was no overt evidence of systemic inflammation in *Il-10$^{-/-}$* mice, and they had comparable body weights and colon morphology to wild-type (WT) controls (Figures S1A–S1C). However, on visual inspection, iWAT from *Il-10$^{-/-}$* mice appeared redder than that from littermate controls. Histological analysis also revealed smaller adipocytes and increased numbers of cells with multilocular lipid droplets (Figure 1A). Serum triglycerides were lower, and serum-free fatty acids were elevated in *Il-10$^{-/-}$* mice (Figure S1D). We further found that *Il-10$^{-/-}$* mice exhibited markedly improved glucose tolerance despite similar basal glucose levels (Figures 1B and S1D). Interestingly, ablation of IL-10 did not have a marked influence on serum pro-inflammatory cytokine levels or total or activated M1 macrophage populations in adipose tissues (Figures S1E and S1F).

Next, we addressed how this phenotype progressed with age. Chow-fed *Il-10$^{-/-}$* mice at 8 months of age were grossly leaner than controls and had less total body mass and fat mass (Figures 1C–1E). Furthermore, the size and weight of individual adipose depots were

reduced (Figure S1G). Livers of *Il-10⁻/⁻* mice also appeared to be protected from hepatic steatosis (Figure 1D). We further assessed how IL-10 ablation would affect the development of diet-induced obesity. Mice of 10 weeks of age were fed a high-fat diet (HFD; 60% calories from fat) for 6 weeks. After this regimen, *Il-10⁻/⁻* mice were grossly leaner and gained less weight than WT mice (Figures 1F and 1G). MRI analysis of body composition confirmed reduced body fat with no difference in lean mass (Figure 1H). *Il-10⁻/⁻* mice were also protected from diet-induced hepatic steatosis, and the size and weight of individual adipose depots were reduced (Figures 1G–1I and S1H). Liver and serum triglyceride and cholesterol levels were reduced in *Il-10⁻/⁻* mice (Figure S1I), and the mice had improved glucose tolerance and insulin tolerance (Figures 1J and 1K). Assessment of AKT phosphorylation in response to insulin suggested that adipose tissue insulin sensitivity was preferentially increased in the absence of IL-10 (Figure S1J).

Colon morphology and histology revealed no apparent signs of colitis in *Il-10⁻/⁻* mice (Figures S1K and S1L), although we noted a small increase in the basal levels of *Mcp1* and *Il-12p40* in colon tissue (Figure S1M). With the exception of IL-10, WT and *Il-10⁻/⁻* mice had comparable levels of most pro-inflammatory cytokines in serum (Figure S1N). There was a modest decrease in both serum and adipose MCP-1 in HFD-fed *Il-10⁻/⁻* mice (Figures S1O and S1P), in line with their protection against diet-induced obesity (Kanda et al., 2006; Sartipy and Loskutoff, 2003).

Increased Energy Expenditure in IL-10-Deficient Mice

Next, we probed the influence of IL-10 expression on energy homeostasis. Chow-fed mice at 10 weeks of age were individually housed in metabolic chambers for 72 hours. Oxygen consumption rate (VO_2) energy expenditure (EE) and food consumption were higher in *Il-10⁻/⁻* mice compared to WT controls (Figures 2A–2C and S2A). Metabolic cage studies performed on an independent cohort of HFD-fed mice revealed similar elevations in VO_2 and EE in mice lacking IL-10 (Figures S2B and S2C).

To examine if the increase in EE in *Il-10⁻/⁻* mice might reflect altered mitochondrial activity, we isolated mitochondria from iWAT and measured rates of oxygen consumption (OCR). Mitochondrial respiration was sequentially measured with substrate present (basal respiration) and in the presence of ADP (complex V respiration) or FCCP (maximal respiration). We observed increases in basal, complex V, and maximal respiration in *Il-10⁻/⁻* mice (Figures 2D and S2D). We then assessed the activity of complexes I-IV by performing an electron flow assay. The activity of all complexes was augmented in *Il-10⁻/⁻* mitochondria (Figures 2E and S2D).

Increased Adipose Thermogenesis in IL-10-Deficient Knockout Mice

To address whether the loss of IL-10 affected adipose gene expression, we performed RNA sequencing (RNA-seq) on iWAT from chow-fed, 10-week-old mice. Remarkably, as depicted in Figure 2F, genes linked to adipocyte thermogenesis were highly upregulated in iWAT from *Il-10⁻/⁻* mice compared to controls. Such genes included *Ucp1*, *Cidea*, and *Pm20d1* (Long et al., 2016). Conversely, genes selectively expressed in WAT and those associated with obesity, including *Mmp12*, *Trem2*, *Celec4d*, and *Atp6v0d2*, were

downregulated. We further analyzed the correlation between the gene expression signatures of WT and *Il-10^{−/−}* iWAT and reference BAT and WAT from public datasets (Seale et al., 2007). The data plot in Figure 2G is divided into four quadrants with different shades of red and blue representing the BAT/WAT ratio as a function of knockout (KO)/WT ratio. The large cluster of genes between the horizontal dotted lines show that vast majority of genes were similarly expressed between WT and KO mice. However, the substantial number of genes clustered in quadrant one indicated that the profile of *Il-10^{−/−}* iWAT more closely resembled BAT than did that of WT. Real-time PCR confirmed that markers of adipose browning were increased in *Il-10^{−/−}* mice, whereas inflammatory markers were reduced or unchanged (Figures 2H and S1O), with the exception of mild increases in the low basal levels of *Tnfa*, *Mcp1*, and *Il-12p40* in colon (Figure S1M). We also found increased UCP-1 protein in adipose tissue of *Il-10^{−/−}* mice (Figure 2I). Expression of previously identified "beige markers" was generally not different, except for a mild enrichment in the TMEM26+ cell population in *Il-10^{−/−}* mice (Figures S2E and S2F). Thermogenic gene expression in BAT was similar between groups (Figure S2G).

To rule out a contribution of subclinical colonic inflammation to the metabolic phenotype of *Il-10^{−/−}* mice, we treated them with the broad-spectrum antibiotic enrofloxacin starting at 4 weeks of age (Hoentjen et al., 2003; Madsen et al., 2000). After 7 weeks of antibiotic *Il-10^{−/−}* mice still had increased adipose thermogenic gene expression (Figure S2H). Thus, the improved metabolic phenotype of *Il-10^{−/−}* mice could not be linked with the development of colitis or obvious systemic inflammation.

Adrenergic signaling is enhanced in mice housed at ambient temperature (23° C) compared to thermoneutrality (30° C). We noted that genes induced in response to cold, such as *Cpn2*, *Otop1*, and *Pm20d1* (Long et al., 2016) were upregulated in *Il-10^{−/−}* mice maintained at 23° C (Figures 2F and 2G). This finding raised the possibility that either increased production of β-adrenergic agonist or increased response to the same level of agonist might contribute to the phenotype of *Il-10^{−/−}* mice. To address this, we housed 4-week-old mice at 30° C for 7 weeks. Thermoneutral housing attenuated the differences in thermogenic gene expression between WT and *Il-10^{−/−}* mice (Figure S2I), suggesting that the phenotype was dependent on active beta-adrenergic signaling. To rule out the possibility that *Il-10^{−/−}* mice were producing more β-adrenergic agonists, perhaps because they were perceiving cold due to changes in skin or fur, we measured body temperature and catecholamine levels and observed no differences between groups (Figures S2J and S2K). Further, *Il-10^{−/−}* mice exposed to cold (5° C) for 6–24 hr showed a more robust increase in thermogenic genes compared to controls (Figure S2L). These findings suggest that *Il-10^{−/−}* affects the downstream response to β-adrenergic agonists.

Bone Marrow IL-10 Production Determines the Thermogenic Phenotype

To determine the source of the IL-10 signal leading to these metabolic effects, we performed bone-marrow transplantation (BMT) studies. We reconstituted lethally irradiated *Il-10^{−/−}* mice with either WT (WT→KO) or *Il-10^{−/−}* bone-marrow (KO→KO) (Figure S3A). Genotyping of blood 7 weeks post-BMT showed that the WT allele was fully reconstituted in *Il-10^{−/−}* mice (Figure S3A). Following the transplant WT→KO mice gained more weight

and accumulated more fat mass than KO→KO controls (Figures 3A and 3B). The iWAT depot was larger in WT→KO mice compared to KO→KO controls (Figure 3C). WT→KO mice also had higher blood glucose levels and were less glucose tolerant (Figures S3B and S3D). Importantly, neither group showed apparent signs of colitis (Figure S3C). We performed calorimetry to investigate whether the thermogenic phenotype of IL-10-deficient mice was rescued by WT bone marrow. WT→KO mice had reduced VO_2 and EE compared to KO→KO mice (Figure 3E). Consistent with this finding, thermogenic gene expression and mitochondrial respiration were repressed in WT→KO mice (Figures 3F–3H and S3D).

IL-10-IL-10R Axis Represses Adipocyte Thermogenesis

To explore if IL-10 could act on adipose tissue directly, we characterized IL-10Rα expression in fat. *Il-10ra* was highly enriched in the mature adipocyte fraction of iWAT and *Il-10ra*, but not *Il-10rb*, was induced during differentiation (Figures 4A, 4B, and S4A). Furthermore, *Il-10ra* was increased in response to HFD, genetic obesity, and aging (Figures 4C and S4B). Interestingly, *Il-10r*α was also regulated over the time course of mice exposed to cold. *Il-10r*α was induced acutely, but fell as thermogenic gene expression increased (Figures S4C and S4D). We also found that cold exposure and HFD feeding led to an increase in serum IL-10 (Figure S4D). IL-10Rα levels were higher in WAT compared to other metabolic tissues such as liver and muscle (Figure S4E).

Meta-analysis of published data from the Metabolic Syndrome in Men (METSIM) study (N = ~10,000) and >100 strains of high-fat/fructose fed mice from the hybrid mouse diversity panel (Laakso et al., 2017; Parks et al., 2013) showed robust correlation of *IL-10Rα* with fat mass and insulin resistance (Figures 4F and 4G). We also identified *Il-10ra* as a direct PPARγ target gene. *Il-10ra* expression was induced in response to PPARγ activation, and analysis of published chromatin immunoprecipitation sequencing (ChIP-seq) data revealed robust enrichment of PPARγ at the enhancer region of the *Il-10ra* gene locus in adipocytes (Figure S4F) (Siersbæk et al., 2012).

Next, we assessed whether the IL-10Rα pathway was functional in adipocytes. We confirmed that IL-10 activated STAT3 phosphorylation (Figure S4G). We then proceeded to knock down IL-10Rα in iWAT with an adenoviral vector expressing a specific small hairpin RNA (shRNA). Partial knockdown of IL-10Rα protein was sufficient to increase thermogenic gene expression (Figures 4D and 4E). We also performed acute knockdown studies *in vivo* using an antisense oligonucleotide (ASO) targeting IL-10Rα . Importantly, we observed knockdown of IL-10Rα expression in fat, but not liver or muscle, in response to ASO treatment (Figure 4H). Acute IL-10Rα depletion by ASO caused weight loss, a reduction in fat but not lean mass, and a reduction in WAT weight (Figures 4I–4K). Neither control ASO-nor IL-10Rα ASO-treated mice showed signs of colitis (Figure S4H). Furthermore, expression of thermogenic genes was increased in iWAT of IL-10Rα ASO-treated mice (Figure 4K).

Treatment of iWAT acutely *ex vivo* with IL-10 decreased UCP1 protein and its corresponding mRNA (Figures 5A and 5B). To establish that these effects were due to direct actions of IL-10 on adipocytes and did not require other cell types, we studied primary beige adipocytes differentiated *in vitro*. Treatment of these cells with IL-10 also led to a robust

downregulation of thermogenic genes (Figure S5A). To facilitate our analysis of IL-10 signaling in cultured adipocytes, we established an immortalized brown-like preadipocyte cell line that expressed IL-10Rα and was capable of inducing thermogenic genes in response to stimuli (iBAd cells). IL-10 signaling was operative in these cells as indicated by induction of the canonical IL-10-responsive gene *Socs3* (Figure 5C). Reciprocal with the induction of *Socs3*, we observed a decrease in *Ucp1* levels and decreased mitochondrial respiration upon IL-10 treatment (Figure S5B). Pretreatment of the cells with an IL-10Rα antibody or small interfering RNA (siRNA)-mediated knockdown of STAT3 blunted the effects of IL-10 (Figures S5C and S5D).

We then assessed global gene expression in differentiating iBAd cells in the presence or absence of IL-10. Genes induced in vehicle-treated cells more than 5-fold on day 5 (D5) of differentiation compared to D0 were plotted as a heat-map (Figure 5D). Thermogenic genes such as *Ucp1*, *Cidea*, and *Pppargc1a* were among the highest induced genes on D5. Moreover, these same genes were also among the most highly inhibited by IL-10 (Figure 5D). Pathway analysis revealed that brown fat cell differentiation and lipid metabolic processes were compromised by IL-10 (Figure 5E). Blockade of the browning program by IL-10 was further validated by plotting the RNA-seq vehicle (NT)/IL-10 expression ratio as a function of WAT/BAT expression ratio (Sun et al., 2013). 70% of the genes inhibited by IL-10 were brown-selective genes, suggesting a high specificity for the browning program (Figure 5F).

IL-10 Alters Chromatin Architecture at Thermogenic Genes

The primary mode of IL-10 action in macrophages is believed to be inhibition of transcription, although the underlying mechanisms are unclear. We found that IL-10 inhibited the abundance of primary transcripts of thermogenic genes and the expression of putative enhancer RNAs (eRNAs) from *Ucp1* (Figure 5G), indicating that IL-10 was acting to block transcription. To test whether IL-10-dependent repression of transcription was due to action at DNA regulatory regions, we performed genome-wide assay for transposase-accessible chromatin sequencing (ATAC-seq) on differentiated iBAd cells. ATAC-Seq peaks correspond to genomic regions sensitive to cleavage by transposase because of their open chromatin configuration (Buenrostro et al., 2013). Using a parallel approach to the RNA-seq analysis of Figure 5D, we identified 3,174 ATAC peaks that were enriched more than 5-fold on D5 compared to D0 in vehicle-treated cells and represented them as a heatmap (Figure 6A). Peaks indicative of open chromatin appearing at D5 included those at the enhancer/promoter regions of thermogenic genes such as *Ucp1 and Cidea*, consistent with the induction of these genes during differentiation. In line with the inhibitory effects of IL-10 on thermogenic gene repression, IL-10 markedly reduced ATAC peak enrichment at thermogenic genes (Figure 6A).

To qualitatively assess the changes in ATAC-seq peaks, we plotted the data as a bedgraph. As shown in Figure 6B, on D5 of brown differentiation a discreet set of new peaks emerged (peaks 1 and 3), indicative of newly opened chromatin at regulatory regions of the *Ucp1* locus. Remarkably, IL-10 treatment caused an almost complete loss of these differentiation-dependent peaks, indicating that the chromatin remained closed in response to IL-10

signaling. These changes in ATAC peaks were consistent with the RNA-seq data showing a decreased *Ucp1* transcript in IL-10-treated cells and increased transcript in IL-10-deficient mice. Importantly, there were a number of prominent ATAC peaks at the *Ucp1* locus that were not affected by IL-10 (e.g., peak 2), indicating that IL-10 was selectively altering chromatin at specific sites (Figure 6B). Specificity was further confirmed by aligning the adipocyte results with ATAC-seq data from *Il-10*$^{-/-}$ bone-marrow-derived macrophages treated with and without IL-10. Most of the peaks present at the *Ucp1* locus in adipocytes were absent in macrophages. ATAC-seq peak quantification at the *Ucp1* locus further validated the repressive effects of IL-10 at peaks 1 and 3, but not 2 (Figure 6C).

IL-10 treatment also altered chromatin configuration at the regulatory regions of a battery of other thermogenic genes, including *Cidea*, *Ppargc1a*, and *Elovl3* (Figures 6B and S6E). Furthermore, examination of ATAC signals at genes whose expression was not altered by IL-10, including *Fabp4 and Ephx1*, showed that the ATAC peaks were virtually unchanged by IL-10 (Figure S5E). The expected increase in ATAC signals at the *Socs3* locus served as a positive control for IL-10 transcriptional effects (Figure S5E). Finally, we plotted the ratio of vehicle/IL-10 from our ATAC-seq data as a function of gene expression (RNA-seq). Changes in ATAC peaks did not always correlate with transcript abundance, suggesting that changes in chromatin configuration do not necessarily translate into transcriptional regulation. However, we found a small cluster of genes in the quadrant 2 of the plot shown in Figure 6D with particularly high ATAC-/RNA-seq correlation. This cluster included thermogenic genes, such as *Ucp1*, *Pppargc1α* , and *Cidea*, further underscoring the specificity of IL-10 action.

To extend our results to beige adipocytes, we performed ATAC-seq on adipocytes differentiated from primary SVFs from iWAT of 10-week-old mice. We found that IL-10 altered chromatin accessibility at thermogenic genes (*Ucp1*, *Cidea*, and *Cox8b*) in primary beige adipocytes (Figure S6A). We isolated mature adipocytes from iWAT and performed ATAC-seq to further establish the physiological relevance of our findings. Consistent with the upregulation of thermogenic genes (Figure 2), regulatory regions of *Ucp1*, *Cidea*, *Cox8b*, *Adrb3*, and *Pm20d1* were in a more open chromatin configuration in *Il-10*$^{-/-}$ compared to WT iWAT adipocytes (Figures 6E, 6F, and S6B). Thus, results from three different models indicated that IL-10 affects chromatin architecture and thermogenic gene transcription in a cell-autonomous manner.

IL-10 Alters Transcription Factor Occupancy at Thermogenic Genes

Thermogenic gene transcription is orchestrated by multiple transcriptional regulators (Harms and Seale, 2013). To investigate if IL-10 affected accessibility at sites of transcription factor binding, we performed *in silico* analysis. We plotted all the ATAC-seq data peaks from D0 and D5 as a function of fold induction to assess the percentage of peaks showing a change in accessibility during differentiation. About 10% of the ATAC peaks show an increase of 5-fold or higher on D5 (SFigure S7A). Furthermore, the distribution of ATAC peaks that were highly enriched during BAT differentiation favored intergenic regions that could possibly contain enhancer elements (Figures S7B and S7C). We separated the ATAC peaks into 10 equivalently sized bins to assess the peak strength (reads per kilobase per million mapped

reads [RPKM]) within each category of samples (D0, D5, and D5+IL-10). Next, we quantitatively assess transcription factor binding sites in the intergenic/enhancer regions where ATAC peaks were enriched. Motifs associated with the binding of canonical thermogenic transcription factors such as CREB/ ATF, C/EBPs, and NFIs were highly enriched on D5 (Figure S7D). By contrast, AP-1 (Fos/Jun) motifs were highly downregulated. To further investigate the effect of IL-10 on transcription factor enrichment, we analyzed the same regions from Figure S7D and divided the motifs into three groups based on the level of IL-10 inhibition. IL-10 caused a substantial loss of enrichment for motifs associated with thermogenesis-linked transcription factors (Figure 7A).

To complement these *in silico* analyses, we directly tested the functional relevance of the transcription factor motifs identified by ATAC-seq. We performed directed qChIP-PCR analysis on the regulatory regions of *Ucp1* gene locus. The boxed peaks in Figure 7D contain sequences that regulate chromatin dynamics through histone modification and recruitment of transcription regulators such as C/EBPs, PGC1α , and CREB/ATF. We found that IL-10 treatment compromised active enhancer histone methylation mark H3K4me1 as well as recruitment of C/EBPβ , PGC1α , and ATF-2 to *Ucp1* regulatory peaks 1 and 3, but not to the constitutively present peak 2 (Figure 7B). In accordance with these ChIP data, IL-10 treatment caused a marked reduction in the ATF-2 phosphorylation and protein levels of PGC1α in adipocytes (Figure 7C).

To further investigate the involvement of C/EBPβ in the actions of IL-10, we performed genome-wide Chip-seq. Motif analysis showed that the C/EBPβ consensus site was highly enriched in our peak analysis, and peak annotation showed that IL-10 treatment did not cause global changes in C/EBPβ DNA occupancy (Figures S7E and S7F). However, gene ontology analysis revealed that IL-10 antagonized C/EBPβ enrichment selectively at gene loci associated with the brown differentiation program (Figure 7D). For example, IL-10 blunted the recruitment of C/EBPβ to regulatory regions of *Elovl6*, *Lpl*, and *Ppargc1a*, without affecting recruitment to *Pparg* (Figures 7E and S7G).

DISCUSSION

Although multiple signaling pathways that can stimulate adipose tissue browning have been characterized, the physiologic limiters of energy expenditure programs are not well defined. Here, we have outlined an unexpected role for IL-10 in the modulation of adipocyte thermogenesis. Loss of IL-10 in mice increased energy expenditure and protected against diet-induced obesity, and did so in the absence of overt systemic or adipose inflammation. We further showed that IL-10 acts directly on adipocytes to repress thermogenic genes by altering the chromatin landscape. These findings expand our understanding of the complexity of regulatory links between immune and inflammatory signaling and adipocyte metabolism. They further suggest that blockade of IL-10 receptor signaling in fat could represent a tractable approach to de-repress thermogenic gene expression in a therapeutic context.

Adipose tissue inflammation is widely regarded to be a contributory factor in the development of metabolic dysfunction (Lumeng and Saltiel, 2011). However, paradoxical

increases in insulin resistance in mice depleted of various pro-inflammatory signals, and the development of age-related obesity upon anti-inflammatory ablation, suggest a more complex relationship between the immune system, adipocytes, and systemic metabolism (Bapat et al., 2015; Wallenius et al., 2002; Wernstedt Asterholm et al., 2014). Several pro-inflammatory molecules have been shown to impair insulin action and lipid storage in mouse models, leading to the suggestion that inhibition of adipose tissue inflammation might be beneficial in the setting of diabetes (Shoelson et al., 2006). Inflammation is also linked with increased energy expenditure in patients with cachexia and inflammatory bowel disease (Barot et al., 1981; Moldawer et al., 1987). The cytokine IL-6 is induced in response to exercise and cancer cachexia has been associated with browning and energy expenditure (Knudsen et al., 2014; Petruzzelli et al., 2014). Similarly, nuclear factor κB (NF-κB) is induced in cancer cachexia and is known to promote energy expenditure (Tang et al., 2010; Tisdale, 1997). In contrast, IL-1β and tumor necrosis factor alpha (TNF-α) have been reported to negatively regulate adipose thermogenesis and to cause desensitization to catecholamines (Goto et al., 2016; Nisoli et al., 2000). Thus, the effects of individual cytokine pathways on thermogenesis are likely to depend on a range of variables, including the source of the cytokine, the duration of the exposure, and the cell type(s) responding to it.

The ability of IL-10 to counter the pro-inflammatory actions of other cytokines is well documented (Saraiva and O'Garra, 2010). Contrary to the expectation that loss of IL-10 might exacerbate adipose inflammation, we did not observe this. Our finding that IL-10-deficient mice had increased thermogenic gene expression even when maintained on an antibiotic that prevents colitis indicates that bowel inflammation is not the driver of their metabolic phenotype. Multiple lines of evidence suggest that adipocyte-intrinsic effects of IL-10 signaling are an important determinant of thermogenesis; however, we acknowledge that we cannot exclude the possibility that secondary changes in the activities of other cytokine pathways might also contribute to the phenotype of IL-10-deficient mice.

Several prior studies have addressed metabolism in IL-10-deficient mice, with differing results. Clementi et al. and den Boer et al. found that *Il-10^{-/-}* mice fed HFD had increased hepatic triglycerides but no change in insulin sensitivity (Clementi et al., 2009; den Boer et al., 2006). In better agreement with our data, Miller et al. (2011) reported that *Il-10^{-/-}* mice fed high fat diet for 12 weeks were protected from hepatic steatosis, and Faulkner et al. (2013) reported that *Il-10^{-/-}* mice on HFD had reduced adiposity and increased insulin sensitivity. Potential factors that might influence these differing results include dietary composition, subtle differences in genetic background of the *Il-10^{-/-}* mice, and vivarium conditions. Given that IL-10 is known to engage in crosstalk with many other pathways, including IL-6 and Toll-like receptor (TLR) signaling, it seems likely that the basal activities of such pathways could also be an important variable in the metabolic consequences of IL-10 deletion.

We have built on prior work in macrophages to dissect the actions of IL-10 in a different cell type, where it acts on a largely distinct set of transcriptional target genes. ATAC- and RNA-seq revealed that chromatin at the regulatory regions of thermogenic genes remained closed during browning in the presence of IL-10. Importantly, this effect was selective for the thermogenic program, as the chromatin structure adipocyte genes not related to browning

was not altered. Thus, IL-10 is not a general inhibitor of adipocyte transcription, but rather a specific modifier of thermogenesis. We also identified specific transcription factors whose interactions with regulatory regions of thermogenic genes were dependent on IL-10 signaling. ATAC accessibility at ATF/CREB and C/EBP motifs was enriched during browning, and the presence of IL-10 antagonized accessibility at these motifs. Consistent with the changes in accessibility at these motifs, directed ChIP analysis showed reduced occupancy of C/EBPβ , ATF-2, and its cofactor PGC-1α at *Ucp1* regulatory regions in the presence of IL-10. Furthermore, genome-wide ChIP-seq analysis revealed selective changes in the recruitment of C/EBPβ to regulatory regions of thermogenic genes. Finally, we found that AFT-2 activation and expression of PGC-1α itself were also repressed in response to IL-10.

Our data are most consistent with the model that IL-10 acts on pre-existing mature adipocytes to enact a change in gene expression that alters their thermogenic activity. IL-10Rα is enriched in white and beige adipocytes and is upregulated during differentiation and in obesity. Thus, hematopoietic-derived IL-10 could act on white adipocytes to maintain adiposity and on beige adipocytes to limit thermogenesis. However, it is also possible that a change in IL-10 signaling might affect the recruitment of beige precursors, especially in a chronic context. For example, in *Il-10$^{-/-}$* mice beige adipocytes could experience sustained adrenergic signaling that would be expected to lead to their maintenance and enrichment (Altshuler-Keylin et al., 2016). We did observe an increase in the frequency of TMEM26+ cells in iWAT of *Il-10$^{-/-}$* mice, although we did not observe robust increases in the expression of classic beige marker genes (Wu et al., 2012). Future lineage tracing studies will be required to directly test the effects of the IL-10 axis on beige progenitor recruitment and expansion.

Our results suggest that IL-10 signaling provides a brake that limits thermogenic gene expression. Since *Il-10ra* is a direct target of PPARγ, it seems reasonable to hypothesize that the IL-10 axis could serve to facilitate lipid storage and maintain adiposity. Given the central role that IL-10 plays in inflammation and immunity, IL-10 signaling might function as a mechanism to conserve energy in the setting of acute systemic demands such as infection. IL-10Rα expression is further elevated in response to obesity and aging, implying that changes in the activity of the IL-10 axis are relevant in these contexts. Finally, our data suggest that blockade of IL-10 signaling in adipose tissue might have beneficial effects in the setting of obesity and insulin resistance. The observation that acute knockdown of IL-10Rα expression in iWAT induces thermogenic gene expression supports further research into the therapeutic utility of targeting the adipose IL-10 axis.

STAR★METHODS

KEY RESOURCES TABLE

REAGENT or RESOURCE	SOURCE	IDENTIFIER
Antibodies		
UCP1	Abcam	Cat# ab10983 RRID:AB_2241462

REAGENT or RESOURCE	SOURCE	IDENTIFIER
PGC1α	Santa Cruz	Cat# sc-13067 RRID:AB_2166218
ATF-2	Santa Cruz	Cat# sc-6233 RRID:AB_2058437
pATF-2	Santa Cruz	Cat# sc-8398 RRID:AB_626709
C/EBPβ	Santa Cruz	Cat# sc-150 RRID:AB_2260363
Tubulin	Millipore	Cat# CP06 RRID:AB_2617116
STAT3	Cell Signaling	Cat# 9139 RRID:AB_331757
pSTAT3 (Tyr705)	Cell Signaling	Cat# 9131 RRID:AB_331586
Actin	Sigma	Cat# A2066 RRID:AB_476693
AKT	Cell Signaling	Cat# 9272 RRID:AB_329827
pAKT (Ser473)	Cell Signaling	Cat# 4060 RRID:AB_2315049
IL10Rα	R&D	AF-474-SP
H3K4ME1	Abcam	Cat# ab8895 RRID:AB_306847
ON-TARGETplus mouse STAT3 siRNA SMARTpool	Dharmacon	L-040794-01-0005
Non-targeting POOL	Dharmacon	D-001810-03-05
CD11b	Tonbo	60-0112-U100
CD11c	Tonbo	35-0114-U100
F4/80	Tonbo	20-4801-U025
TMEM26	Imgenex	IMG-6633A
DAPI	Molecular Probes	D1306
B220	BD Bioscience	561880
Ter119	eBioscience	25-5921-81
CD137	eBioscience	12-1371-81
IL10Rα generation 2.5 antisense oligonucleotide (ASO)	Ionis Pharmaceutical	939570
DMEM	Corning	MT-10-013-CM
FBS	Omega Scientific	FB11
DMEM/F12 Glutamax	Thermo Fischer	10565-018
Trypsin	Corning	MT-25-053-CI
Penicillin/Streptomycin	Corning	MT-30-002-CI
Lipofectamine 2000	Thermo Fischer	11668027
Bacterial and Virus Strains		
Adenovirus: IL10Rα shRNA	This paper	N/A
Retrovirus: IL10Rα	This paper	N/A
Chemicals, Peptides, and Recombinant Proteins		
3-isobutyl-1-methylxanthine	Sigma	I-7018
Dexamethasone	Sigma	D-2915
Rosiglitazone	Sigma	R-2408
T3 (3,3′,5-Triiodo-L-thyronine)	Sigma	T-2877
Isoproterenol	Sigma	I-6504

REAGENT or RESOURCE	SOURCE	IDENTIFIER
Forskolin	Sigma	F3917
Indomethacin	Sigma	I-7378
REAGENT or RESOURCE	SOURCE	IDENTIFIER
Insulin	Thermo Fischer	12585-014
Recombinant mouse IL10	Peprotech	210-10
Glucose	Sigma	G8769-100ML
Adenosine	Sigma	A9251-1G
Ascorbic acid	Sigma	A4544
Electrophoresis grade delipidated BSA	Sigma	A7030
Sodium Metabisulfite	Sigma	S9000
Collagenase D	Roche	11088882001
Collagenase B	Roche	11 088 831 001
Dispase II	Roche	04942078001
Enroflox® 100 (Enrofloxacin)	Norbrook	NDC-55529-152-04
Red Blood Cell (RBC) lysis buffer	Sigma	R7757
Humulin® R U-100 (Human Insulin for ITT)	Lilly	002-8215-01
Puromycin	Sigma	P9620
Hygromycin	Sigma	H0654
Polybrene	Millipore	TR-1003-G
RIPA buffer	Boston BioProducts	BP-115-500ml
IsoFlo (Isoflurane)	Zoetis	N/A
Formalin	Fischer	23-305-510
Critical Commercial Assays		
TruSeq Stranded Total RNA Library Prep Kit	Illumina	RS-122-2102
Nextera Tn5 Transposase kit	Illumina	FC-121-1030
Kapa LTP Library Preparation Kit	KR0453	KR0453
Wako L-Type Triglyceride Assay M Enzyme Color A	Wako	461-08992
Wako NEFA-HR	Wako	991-34891
Wako Cholesterol E Test	Wako	439-17501
Milliplex Kit	Millipore	MCYTOMAG-70K-09 M
3-CAT Research ELISA	Rocky MTN Diagnositics	BA E-5600
BCA protein assay kit	Pierce	23225
Vectastain Elite ABC kit	Vectastain	PK-6100
Deposited Data		
All sequencing data	This paper	GEO: GSE94654
Experimental Models: Cell Lines		
iWAT primary preadipocytes	This paper	N/A
iWAT immortalized preadipocytes	This paper	N/A
BAT immortalized preadipocytes	This paper	N/A

REAGENT or RESOURCE	SOURCE	IDENTIFIER
iBAd-BAT immortalized preadipocytes expressing IL10Rα	This paper	N/A
Phoenix-ECO cells (Retrovirus packaging)	ATCC	CRL-3214
Experimental Models: Organisms/Strains		
Mouse: *Il10*^{−/−}: B6129P2-*Il10*[tm1cgn]/J	Jackson Lab	02251
Mouse: WT: C57BL/6J	Jackson Lab	000664
Oligonucleotides		
Mouse qPCR Primers, see Table S1	N/A	N/A
ChIP-qPCR Primers, see Table S2	N/A	N/A
CACCGGGCCAGCTGTATAGACATCTC	This paper	N/A
GAAAGATGTCTATACAGCTGGCCC-Lacz shRNA		
CACCGCATCTTAGTCATATCTATGCCGAA GCATAGATATGACTAAGATGC- IL10Rα shRNA	This paper	N/A
Recombinant DNA		
pENTR/U6 plasmid IL10Rα	This paper	N/A
pBLOCK-IT adenovirus vector IL10Rα shRNA	This paper	N/A
Retroviral pBABE-puro IL10Rα	This paper	N/A
pENTR223.1 mouse IL10Rα	Harvard Plasmids	MmCD00081028
Software and Algorithms		
Prism6	GraphPad	N/A
ImageJ	https://imagej.nih.gov/ij/	N/A
HOMER	http://homer.ucsd.edu/homer/	N/A
MACS2	http://liulab.dfci.harvard.edu/MACS/Download.html	N/A
Pscan	http://159.149.160.88/pscan/	N/A
Samtools	https://github.com/samtools/samtools	N/A
SeqMonk	https://www.bioinformatics.babraham.ac.uk/projects/seqmonk/	N/A
Bowtie2	http://bowtie-bio.sourceforge.net/bowtie2/index.shtml	N/A
Tophat	http://tophat.cbcb.umd.edu	N/A
Bioconductor DESeq2	http://bioconductor.org/packages/release/bioc/html/DESeq.html	N/A
MS Excel 2016	Microsoft	N/A
Other		
High Fat Diet (HFD; 60% kcal fat)	Research Diets	N/A
TissueLyzer	QIAGEN	N/A
Metabolic Chamber-Comprehensive	Columbus Instruments	N/A
Lab Animal Monitoring System (CLAMS)		
Mouse MRI machine	EchoMRI	N/A
FACS machine	BD Bioscience	BD FACSVERSE
Applied Biosystem (ABI) qPCR machine	Thermo Fischer	QuantStudio 6 Flex System
100 µm cell strainer	Falcon	352360
70 µm cell strainer	Falcon	352350

REAGENT or RESOURCE	SOURCE	IDENTIFIER
BioCoat 6-well collagen I plate	Fisher	08-772-69
Syber Green Master Mix	Diagenode	DMMLD2D600

CONTACT FOR REAGENT AND RESOURCE SHARING

Further information and requests for resources and reagents should be directed to and will be fulfilled by the Lead Contact, Peter Tontonoz (ptontonoz@mednet.ucla.edu).

EXPERIMENTAL MODEL AND SUBJECT DETAILS

Mice—Breeding pairs of $Il10^{-/-}$ mice and WT controls were acquired from Jackson Laboratory and colony maintained in pathogen-free barrier-protected environment (12:12 h light/dark cycle, 22° C–24° C) at UCLA animal facility. Experimental mice were sacrificed at ages mentioned in figure legends for histological, protein, and gene expression analysis. All the mutant strains used in this study were backcrossed to a C57BL/6 background as stated by Jackson inventory. Animal experiments were conducted in accordance with the UCLA Institutional Animal Care and Research Advisory Committee.

Cell Culture—Murine white and brown preadipocytes were cultured in Dulbecco's modified Eagle's medium (DMEM) supplemented 10% fetal bovine serum (FBS). For *in vitro* brown/beige adipocyte differentiation, preadipocytes were grown to confluence in DMEM with 10% FBS plus insulin (5 μg/ml) and T3 (1 nM). Confluent cells were induced to differentiate with dexamethasone (1 μM), IBMX (0.5 mM), insulin (5 μg/ml), indomethacin (125 nM) and Rosiglitazone (1 μM) for 2 days, followed by insulin, T3 and Rosiglitazone alone. On the fourth day, cells were pretreated for overnight (~16h) with and without 100 ng/ml IL10 and next day treated with 10 μM isoproterenol or forskolin for 5–6 h. White and brown preadipocytes were isolated and immortalized as previously described (Villanueva et al., 2013) and below. Brown preadipocytes IL10Rα expressing stable cells (iBAD) were generated using the pBabe retroviral system (Hummasti and Tontonoz, 2006) and described below.

METHOD DETAILS

Bone marrow transplantation studies—Ten week old $Il10^{-/-}$ mice (n = 3–4) were euthanized using isoflurane. Mice were dunked in 70% EtOH and fur/skin was removed from legs. Quadriceps and hamstring were removed to expose pelvic joints. Hair and muscles were removed and legs were kept in ice-cold PBS during processing of other legs. Tissues were then removed from legs to expose tibia and femur. After all the legs were collected, tibiae and femurs were separated and kept in PBS/DMEM solution. Bones were picked with forceps and using 23G subQ gauge needles PBS/DMEM solution was pushed through to oust bone marrow onto 2–3ml DMEM solution on a Petri dish. Using 18 gauge needles bone marrow chunks were broken apart by gently aspirating. Bone marrow solution was strained onto 50 mL conical tube using cell strainer (70 μm) to remove any debris. Petri dish was rinsed with 1–2 mL PBS/DMEM to collect residual bone marrow. The solution was spun down for 5 min at room temperature (RT) at 1200 rpm. RBC lysis buffer was added to

the pellet for 5min and spun down again. Pellets were washed three times and bone marrow cells were counted and stored on ice for later injection into recipient mice. For bone marrow transplantation (BMT) studies, recipient WT or *Il10*^{−/−} mice (10 weeks of age) were lethally irradiated with 900 rads and transplanted with 3×10^6 bone marrow cells from above donor mice (*Il10*^{−/−}) via tail vein injection. After injection mice were place in immunocompormised room in autoclaved cages supplemented with sterilized water and chow feed. Mice were kept on antibiotics regiment (see below) for 6 weeks and then moved to experimental facility and maintained in normal chow diet. Mice weights and body composition were measured every week. Mice were subjected to metabolic studies as indicated in figures and figure legends.

Antibiotic Treatment—Antibiotic treatment was performed as previously described (Hoentjen et al., 2003; Madsen et al., 2000) with modifications. Weaned (3 week old) WT or *Il10*^{−/−} mice were treated with 660 mg/L broad spectrum antibiotic enrofloxacin (Enroflox® 100, Norbrook, equivalent to ciprofloxacin). Antibiotic was added to drinking water every week for 7 weeks dosed at ~100 mg/kg/day.

Cold exposure studies—For 4° C cold exposure experiment, WT or *Il10*^{−/−} mice at 8–10 weeks of age were singly or doubly housed at 4°C room in a non-bedded cage with access to food and water for the time points indicated in figure legend. At the end of the experiment, iWATs were resected for gene expression analysis.

Thermoneutral condition studies—For thermoneutral experiment, WT and *Il10*^{−/−} mice at 4 weeks of age were housed (4/cage with bedding) in 30°C room with 12h light:dark cycle for 7 weeks on a regular chow diet. After 7 weeks, various tissues including iWATs were resected for gene analysis.

High fat diet studies—For diet study, 10 weeks of age *Il10*^{−/−} and WT mice were fed a 60% high-fat diet (Research Diets) for the indicated times. Mice weights and body composition were measured every week and food was replaced weekly.

Cytokines and Lipid Measurement—On the day of harvest, mice were fasted for 6 h and euthanized using isoflurane Blood was drawn by cardiac puncture and kept in clot activator commercial tube (Terumo CAPIJET, T-MG) and placed on ice. Blood was spun down at 8000 rpm for 5 mins at 4°C table-top centrifuge and serum was collected and stored at −80° C. Liver lipids were isolated using Folch extraction method and as previously described (Sallam et al., 2016). Serum cytokines were measured using Milliplex mouse cytokine Magnetic kit (Millipore) and serum lipids were measured using Wako L-Type TG M, Wako NEFA-HR, or Wako Cholesterol E Test kit according to manufactures' instructions.

Serum and Adipose Catecholamine Measurement—Serum samples were collected as described above. Adipose tissue homogenates were collected as previously described (Qiu et al., 2014). Briefly, resected adipose tissues were flash frozen in liquid nitrogen and stored at −80°C until further analysis. 600 μL of homogenization buffer (0.01N HCl, 1mM EDTA, 4mM $Na_2S_2O_5$) was added to 100–300 mg of tissue and were homogenized using

TissueLyzer for 1min at 30 MHz. Cellular debris was cleared by centrifugation at 13000 rpm for 15 min at 4°C. 50 μL of serum and 200 μL of cleared adipose homogenate was used to measure catecholamine levels using 3-CAT Research ELISA (Labor Diagnostika Nord GmBH & Co.) according to manufacturer's instructions.

Measurement of Core Temperature—Core body temperature of WT and $Il10^{-/-}$ mice was measured at room temperature using rectal probe (BAT-10) purchased from Physitemp.

Glucose Tolerance Test (GTT) and Insulin Tolerance Test (ITT)—For glucose tolerance tests, mice were fasted for 6 h and challenged with an intraperitoneally (i.p.) injection of glucose (2 g/kg). For insulin tolerance tests, mice were fasted for 6 hr and given an i.p. injection of insulin (1 U/kg). Blood glucose levels were monitored using the ACCUCHEK active glucometer (Roche) at times indicated in figure legends.

Indirect Calorimetry and Body Composition Measurements—Indirect calorimetry was performed using a Columbus Instruments Comprehensive Lab Animal Monitoring System (CLAMS, Columbus Instruments). Animals were placed individually in chambers for 3 consecutive days at ambient temperature (26.5°C) with 12 hr light/dark cycles. Animals had free access to food and water. Respiratory measurements were made in 20 min intervals after initial 7–9 hr acclimation period. Energy expenditure was calculated from VO2 and RER using the Lusk equation, EE in Kcal/hr = (3.815 + 1.232 X RER) X VO2 in ml/min. Food intake was measured in metabolic chambers. Body composition (fat and lean mass) was determined using EchoMRI Body Composition Analyzer

***Ex vivo* iWAT IL10 treatment**—For *ex vivo* iWAT IL10 treatment, 10 week old WT mice were housed at cold room (4–6°C) for 6 h and iWATs were isolated and minced, placed in KREB's Ringer Buffer (12 mM HEPES, 121 mM NaCl, 4.9 mM KCl, 1.2 mM $MgSO_4$, 0.33 mM $CaCl_2$) supplemented with 0.1% glucose and incubated with and without 100 ng/ml IL10 for 30 mins-1h at 37°C.

Construction of Adenovirus (Ad) expressing IL10Rα shRNA—Invitrogen's Gateway cloning strategy was used to generate mouse IL10Rα shRNA adenovirus. shRNA targeting mouse IL10Rα was designed using Invitrogen Block-iT RNAi Designer. Forward and reverse shRNA oligonucleotides were synthesized by Integrated DNA Techonologies (IDT) and diluted to 200 uM and annealed and ligated into gateway entry plasmid pENTR/U6 vector (Invitrogen). To generate mammalian expression constructs, we used LR recombination between IL10Rα containing pENTR/U6 and pAD-BLOCK-iT to generate AD-shIL10Rα . Viruses were amplified, purified, and tittered by Viraquest.

Adenovirus IL10Rα shRNA injection into iWAT—For the IL10Rα shRNA adenovirus delivery to fat pads, $2X10^9$ PFU of adenovirus was percutaneously injected into each inguinal fat depot of anesthetized WT mice at 8–10 weeks of age. In each mouse, Ad-IL10Rα shRNA was injected into iWAT on one side, and Ad-Lacz shRNA (control) was injected into the contralateral side as a control. 4–5 days after the injection, iWATs were resected for gene expression analysis.

Acute IL10Rα antisense oligonucleotide (ASO) studies—For acute ASO studies, WT mice at 8–10 weeks of age were i.p. injected with control or IL10Rα ASO (CCTTTCTACAGATATG) at 25mg/kg for twice a week for 3 weeks. Body weight was measured weekly and body composition was determined by EchoMRI analysis. At the end of ASO treatment, various tissues were resected and weighted and subjected to gene expression analysis.

Tissue hematoxylin and eosin (H&E) staining and immunohistochemistry— Tissues (4–5 microns thickness) were placed in cassettes and submerged in 10% formalin solution overnight. Tissue cassettes were washed with tap water for 15 minutes and stored in 70% EtOH at room temperature. Paraffin embedment and H&E staining was performed at the Translational Pathology Core Laboratory (TPCL) at UCLA. Vectastain Elite ABC kit was used for UCP1 and MCP1 immunohistochemistry as per manufacturer's instructions.

Cellular and Mitochondrial Respiration assay—Cell were seeded in a XF24 plate, differentiated, and analyzed in a XF24 analyzer (Seahorse Bioscience/Agilent) as described (Wu et al., 2007). Briefly, oxygen consumption rate (OCR) was measured before and after the sequential injection of 0.75 μM oligomycin, 1 μM FCCP, and 1 μM of rotenone/ myxothiazol. Mixing, waiting, and measurement times were 5, 2, and 2 min, respectively. Measures were normalized by total protein. In another set of experiments, mitochondria were isolated from fresh tissues and immediately used in a XF24 analyzer as previously described (Rogers et al., 2011). Briefly, mitochondria were isolated in MSHE+BSA buffer using a 800 g/8000 g dual centrifugation method and resuspended in MAS buffer. Protein concentration was determined using a Bradford Assay reagent (Bio-Rad) and 20 μg of protein were seeded per well by centrifugation. Coupling and electron flow assays were performed as described (Rogers et al., 2011). For the coupling assay, basal oxygen consumption rate (OCR) was measured in the presence of 10 mM succinate and 2 μM rotenone, and after sequential addition of 4 mM ADP (Complex V substrate), 2.5 μg/ml oligomycin (Complex V inhibitor), 4 μM FCCP (mitochondrial uncoupler) and 4 μM antimycin A (Complex III inhibitor). Coupled respiration was calculated as the difference between basal and response to oligomycin. Uncoupled respiration was the difference between oligomycin and antimycin A injections. For electron flow assays, basal OCR was measured in presence of 10 mM pyruvate (Complex I substrate), 2 mM malate and 4 μM FCCP, and after sequential addition of 2 μM rotenone (Complex I inhibitor), 10 mM succinate (Complex II substrate), 4 μM antimycin A (Complex III inhibitor) and 1mM TMPD containing 10 mM ascorbate (Complex IV substrate). Complex III respiration corresponds to the antimycin A-sensitive respiration.

Construction of immortalized beige/brown preadipocytes expressing IL10Rα (iBAd) cells—Mouse IL10Rα in gateway cloning vector pENTR223.1 was purchased from Harvard Plasmids. To generate mammalian expression construct, pENT223.1 mIL10Rα was LR recombined into gateway retrovirus vector pBabe-puro. pBABE-mIL10Rα was transfected into retrovirus packaging Pheonix E cells for 48hrs. Target cells (immortalized beige/brown preadipocytes) were plated at 50% confluency 24hrs post-transfection. 48 h after transfection media from transfected Phoenix-E cells were harvested and spun down for

5min at 5000 rpm to pellet cells and debris. Retrovirus containing supernatant was carefully removed and plated onto target cells with 1:1000 polybrene for overnight. Next day, media was replaced with regular growth media and cells were incubated for additional 24 h. 4.5 μg/ml puromycin selection was performed to select for cells stably expressing mIL10Rα .

Isolation of and immortalization of primary white and brown adipocytes—Male mice (8–10 week old) were euthanized in isoflurane chamber. Mice were sprayed thoroughly with 70% EtOH. 100–300 mg of inguinal WAT (iWAT) or BAT were dissected and placed on sterile 6-well tissue culture plate with ice-cold 1XPBS. Fat pads were blotted on a napkin to removed excess liquid. Tissues were cut with scissors and minced using blade. Minced fat pads (600–800 mg) were placed in a15ml conical tube containing 3 mL of digestion buffer (PBS, 1.5 U/ml Collagenase D (iWAT) or collagenase B (BAT), 2.4 U/ml Dispase II, 10 mM CaCl$_2$) and incubated at 37°C for 45 min with gentle shaking. Inside tissue culture hood, 10–15 mL of plating media DMEM/F12 with glutamax supplemented with 15%FBS and 1% pen/strep was added to digested solution and slowly resuspended 5 times. The digestion mixture was passed through 100 μm cell strainer and centrifuged at 500 x g for 10 mins at room temperature. Supernatant was carefully decanted and pellet resuspended in 10 mL of plating media and passed through 40 μm cell strainer. Filtered suspension was spun down again at 500 x g for 10 mins at room temperature. Supernatant was decanted and pellet resuspended in 6ml plating media and plated onto collagen-coated plates. After overnight incubation, media was changed every other day until the cells reached 70% confluency (−3–4 days post-harvest). White and brown stromal vascular fractions (SVF) were with differentiated into beige/brown adipocytes using protocol mentioned above or immortalized. For immortalization, retrovirus-expressing largeT-antigen in pBABE-hygromycin vector was generated as mentioned above. Virus was added to target cells and selected with 600 μg/ml hygromycin to make immortalized cells.

ATAC-Seq in cells—ATAC-Seq libraries were prepared from 100,000 cells using the Nextera Tn5 Transposase and DNA library preparation kit (Illumina) as described (Buenrostro et al., 2015) with slight modifications. Libraries were single-end sequenced (50bp) on an Illumina HiSeq 2000. Reads were mapped to the mouse genome (NCBI37/mm9) using Bowtie2. Reads were removed from the subsequent analysis if they were duplicated, mapped to mitochondrial genome, or aligned to unmapped contiguous sequences. Peak calling was performed using MACS2 using parameters callpeak–nomodel -g mm–keep-dup all -q 0.01–llocal 10000. The reads were converted to reads per thousand base pairs peak per million mapped reads (RPKM) by dividing by the total number of reads per sample.

ATAC-Seq in mature adipocytes—Adipocyte nuclei isolation from chow-fed 10 week old WT and *Il10*$^{-/-}$ mice was performed as previously described with modifications (Church et al., 2014). WT and *Il10*$^{-/-}$ mice iWAT (~100–200 mg) was isolated and minced and digested in Krebs Ringer Henseleit Buffer (1M HEPES, 2M NaCl, 1 M KCL, 1 M CaCl$_2$, 1 M MgCl$_2$, 1M K$_2$HPO4, pH 7.4) supplemented with 5mM glucose, 0.1 μM adenosine, 0.1 mg/ml ascorbic acid, 4% electrophoresis grade delipidated BSA and collagenase D for 45 mins saking at 180 rpm at 37°C. Adipocyte suspension were filtered through 100 μm nylon

mesh and washed with buffer. 250,000 cells from the filtered adipocyte suspension were subjected to ATAC-Seq procedure as described above.

RNA-Seq—Total RNA was prepared as described (Tong et al., 2016). Strand-specific libraries were generated from 500 ng total RNA using the TruSeq Stranded Total RNA Library Prep Kit (Illumina). cDNA libraries were single-end sequenced (50bp) on an Illumina HiSeq 2000 or 4000. Reads were aligned to the mouse genome (NCBI37/mm9) with TopHat v1.3.3 and allowed one alignment with up to two mismatches per read. mRNA RPKM values were calculated using Seqmonk's mRNA quantitation pipeline. All RPKMs represent an average from three biological replicates for in-vitro studies, and pooled RNA representation for tissue samples where equal amounts of RNA were pooled from 11 $Il10^{-/-}$ animals and 9 WT animals prior to library construction. A gene was included in the analysis if it met all of the following criteria: The maximum RPKM reached 4 at any time point, the gene length was > 200bp, and for in-vitro studies was induced at least 3-fold from Day 0 samples, and the expression was significantly different from the basal ($p < 0.01$) as determined by the DESeq2 package in R Bioconductor. P values were adjusted using the Benjamini-Hochberg procedure of multiple hypothesis testing (Benjamini and Hochberg, 1995).

Chromatin immunoprecipitation (ChIP) and ChIP-Seq—ChIP experiments were performed according to standard protocols (Villanueva et al., 2011, 2013). Lysed cells were sonicated using a Bioruptor (Diagenode) according to the manufacturer's protocol, and chromatin was immunoprecipitated with antibodies against PGC1α (H-300 sc-13067, Santa Cruz Biotechnology), ATF-2 (C-19 sc-187, Santa Cruz Biotechnology), C/EBPβ (sc-150, Santa Cruz Biotechnology), and IgG (PP64, Millipore) overnight at 4°C in the presence of Protein A beads (GE Healthcare). DNA enrichment was quantified by real-time PCR (ABI QuantStudio) using SYBR Green Master Mix (Diagenode). Primers used for these studies are list in Table S2. Occupancy was quantified using a standard curve and normalized to input DNA. ChIP-Seq libraries were prepared using the Kapa LTP Library Preparation Kit (Kapa Biosystems). ChIP-Seq was performed as described (Tong et al., 2016). Reads were aligned to the mouse genome (NCBI37/mm9) with Bowtie2. Uniquely mapped reads were used for peak calling and annotation using HOMER (Heinz et al., 2010). Peaks were called if they passed a false discovery rate of 0.01 and were enriched over input. Peaks were annotated to the nearest TSS.

Gene Expression Analysis—Total RNA was isolated using TRIzol reagent (Invitrogen) and reverse transcribed with the iScript cDNA synthesis kit (Biorad). cDNA was quantified by real-time PCR using SYBR Green Master Mix (Diagenode) on an ABI QuantStudio instrument. Gene expression levels were determined by using a standard curve. Each gene was normalized to the housekeeping gene 36B4 and was analyzed in duplicate. Primers used for real-time PCR are listed in Table S1.

Protein Analysis—Whole cell lysate or tissue lysate was extracted using RIPA lysis buffer (Boston Bioproducts) supplemented with complete protease inhibitor cocktail (Roche). Proteins were diluted in Nupage loading dye (Invitrogen), heated at 95°C for 5

min, and run on 4–12% NuPAGE Bis-Tris Gel (Invitrogen). Proteins were transferred to hybond ECL membrane (GE Healthcare) and blotted with commercial antibodies mentioned in the figure legends and the Key Resources Table.

Mouse and human population-based investigation of IL10Rα—Hybrid mouse diversity panel data was analyzed from 106 inbred strains fed a High-fat high-sucrose diet for 8 weeks as previously described (Parks et al., 2013, 2015). Mouse adipose tissue global expression was analyzed using Affymetrix HT_MG430A arrays and overlaid with phenotypic measurements. Human adipose tissue expression arrays using Affymetrix U219 microarray and phenotypic data was analyzed from the Metabolic Syndrome in Men (METSIM) study (Laakso et al., 2017; Stancákováet al., 2009). All correlations were assessed from the midweight bicorrelation coefficient and corrected p value using the R package WGCNA (Langfelder and Horvath, 2008).

QUANTIFICATION AND STATISTICAL ANALYSES

Motif Analysis—MACS2 called ATAC peak regions were used for motif analysis. JASPAR2016 Position Weight Matrices were used to identify binding sites in ChIP-Seq and ATAC peaks using Pscan-ChIP (Zambelli et al., 2009)

Statistics—All data are presented as mean ± SEM and analyzed using Microsoft Excel and Prism (Graphpad). Student's t test was used for single variable comparison between two groups. One-way ANOVA followed by Dunnett post hoc test was used for multiple comparisons versus the control group. Two-way ANOVA followed by Bonferroni posttests was used to examine interactions between multiple variables. Statistical significance for CLAMS study was determined by using two-way ANOVA repeated-measures and multiple regression analysis (ANCOVA). Data are presented as ± SEM $p < 0.05$ was considered to be statistically significant and is presented as * $p < 0.05$, ** $p < 0.01$, *** $p < 0.001$, or **** $p < 0.0001$.

DATA AND SOFTWARE AVAILABILITY

The accession number for the genome-wide sequencing dataset reported in this paper is GEO: GSE94654

Supplementary Material

Refer to Web version on PubMed Central for supplementary material.

Acknowledgments

References

Altshuler-Keylin S, Shinoda K, Hasegawa Y, Ikeda K, Hong H, Kang Q, Yang Y, Perera RM, Debnath J, Kajimura S. Beige adipocyte maintenance is regulated by autophagy-induced mitochondrial clearance. Cell Metab. 2016; 24:402–419. [PubMed: 27568548]

Bapat SP, Myoung Suh J, Fang S, Liu S, Zhang Y, Cheng A, Zhou C, Liang Y, LeBlanc M, Liddle C, et al. Depletion of fat-resident Treg cells prevents age-associated insulin resistance. Nature. 2015; 528:137–141. [PubMed: 26580014]

Barot LR, Rombeau JL, Steinberg JJ, Crosby LO, Feurer ID, Mullen JL. Energy expenditure in patients with inflammatory bowel disease. Arch Surg. 1981; 116:460–462. [PubMed: 7213002]

Benjamini Y, Hochberg Y. Controlling the false discovery rate: a practical and powerful approach to multiple testing. J R Stat Soc Series B. 1995; 57:289–300.

Buenrostro JD, Giresi PG, Zaba LC, Chang HY, Greenleaf WJ. Transposition of native chromatin for fast and sensitive epigenomic profiling of open chromatin, DNA-binding proteins and nucleosome position. Nat Methods. 2013; 10:1213–1218. [PubMed: 24097267]

Buenrostro JD, Wu B, Chang HY, Greenleaf WJ. ATAC-seq: a method for assaying chromatin accessibility genome-wide. Curr Protoc Mol Biol. 2015; 109(21):29.1–9. [PubMed: 25559105]

Church CD, Berry R, Rodeheffer MS. Isolation and study of adipocyte precursors. Methods Enzymol. 2014; 537:31–46. [PubMed: 24480340]

Clementi AH, Gaudy AM, van Rooijen N, Pierce RH, Mooney RA. Loss of Kupffer cells in diet-induced obesity is associated with increased hepatic steatosis, STAT3 signaling, and further decreases in insulin signaling. Biochim Biophys Acta. 2009; 1792:1062–1072. [PubMed: 19699298]

Couper KN, Blount DG, Riley EM. IL-10: the master regulator of immunity to infection. J Immunol. 2008; 180:5771–5777. [PubMed: 18424693]

den Boer MA, Voshol PJ, Schröder-van der Elst JP, Korsheninnikova E, Ouwens DM, Kuipers F, Havekes LM, Romijn JA. Endogenous interleukin-10 protects against hepatic steatosis but does not improve insulin sensitivity during high-fat feeding in mice. Endocrinology. 2006; 147:4553–4558. [PubMed: 16709607]

Faulkner JL, Gomolak JR, Didion SP. Interleukin-10 deficiency limits the development of obesity and insulin resistance produced by a high fat diet. FASEB J. 2013; 27(Suppl 1):1183.6.

Feldmann HM, Golozoubova V, Cannon B, Nedergaard J. UCP1 ablation induces obesity and abolishes diet-induced thermogenesis in mice exempt from thermal stress by living at thermoneutrality. Cell Metab. 2009; 9:203–209. [PubMed: 19187776]

Gao M, Zhang C, Ma Y, Bu L, Yan L, Liu D. Hydrodynamic delivery of mIL10 gene protects mice from high-fat diet-induced obesity and glucose intolerance. Mol Ther. 2013; 21:1852–1861. [PubMed: 23774795]

Goto T, Naknukool S, Yoshitake R, Hanafusa Y, Tokiwa S, Li Y, Sakamoto T, Nitta T, Kim M, Takahashi N, et al. Proinflammatory cytokine interleukin-1β suppresses cold-induced thermogenesis in adipocytes. Cytokine. 2016; 77:107–114. [PubMed: 26556104]

Harms M, Seale P. Brown and beige fat: development, function and therapeutic potential. Nat Med. 2013; 19:1252–1263. [PubMed: 24100998]

Heinz S, Benner C, Spann N, Bertolino E, Lin YC, Laslo P, Cheng JX, Murre C, Singh H, Glass CK. Simple combinations of lineage-determining transcription factors prime cis-regulatory elements required for macrophage and B cell identities. Mol Cell. 2010; 38:576–589. [PubMed: 20513432]

Hoentjen F, Harmsen HJ, Braat H, Torrice CD, Mann BA, Sartor RB, Dieleman LA. Antibiotics with a selective aerobic or anaerobic spectrum have different therapeutic activities in various regions of the colon in interleukin 10 gene deficient mice. Gut. 2003; 52:1721–1727. [PubMed: 14633949]

Hong EG, Ko HJ, Cho YR, Kim HJ, Ma Z, Yu TY, Friedline RH, Kurt-Jones E, Finberg R, Fischer MA, et al. Interleukin-10 prevents diet-induced insulin resistance by attenuating macrophage and cytokine response in skeletal muscle. Diabetes. 2009; 58:2525–2535. [PubMed: 19690064]

Hummasti S, Tontonoz P. The peroxisome proliferator-activated receptor N-terminal domain controls isotype-selective gene expression and adipogenesis. Mol Endocrinol. 2006; 20:1261–1275. [PubMed: 16556736]

Kanda H, Tateya S, Tamori Y, Kotani K, Hiasa K, Kitazawa R, Kitazawa S, Miyachi H, Maeda S, Egashira K, Kasuga M. MCP-1 contributes to macrophage infiltration into adipose tissue, insulin resistance, and hepatic steatosis in obesity. J Clin Invest. 2006; 116:1494–1505. [PubMed: 16691291]

Keubler LM, Buettner M, Häger C, Bleich A. A Multihit model: colitis lessons from the interleukin-10-deficient mouse. Inflamm Bowel Dis. 2015; 21:1967–1975. [PubMed: 26164667]

Knudsen JG, Murholm M, Carey AL, Biensø RS, Basse AL, Allen TL, Hidalgo J, Kingwell BA, Febbraio MA, Hansen JB, Pilegaard H. Role of IL-6 in exercise training- and cold-induced UCP1 expression in subcutaneous white adipose tissue. PLoS ONE. 2014; 9:e84910. [PubMed: 24416310]

Kowalski GM, Nicholls HT, Risis S, Watson NK, Kanellakis P, Bruce CR, Bobik A, Lancaster GI, Febbraio MA. Deficiency of haematopoietic-cell-derived IL-10 does not exacerbate high-fat-diet-induced inflammation or insulin resistance in mice. Diabetologia. 2011; 54:888–899. [PubMed: 21210076]

Laakso M, Kuusisto J, Stancaáková A, Kuulasmaa T, Pajukanta P, Lusis AJ, Collins FS, Mohlke KL, Boehnke M. The Metabolic Syndrome in Men study: a resource for studies of metabolic and cardiovascular diseases. J Lipid Res. 2017; 58:481–493. [PubMed: 28119442]

Lang R, Patel D, Morris JJ, Rutschman RL, Murray PJ. Shaping gene expression in activated and resting primary macrophages by IL-10. J Immunol. 2002; 169:2253–2263. [PubMed: 12193690]

Langfelder P, Horvath S. WGCNA: an R package for weighted correlation network analysis. BMC Bioinformatics. 2008; 9:559. [PubMed: 19114008]

Lee MW, Odegaard JI, Mukundan L, Qiu Y, Molofsky AB, Nussbaum JC, Yun K, Locksley RM, Chawla A. Activated type 2 innate lymphoid cells regulate beige fat biogenesis. Cell. 2015; 160:74–87. [PubMed: 25543153]

Long JZ, Svensson KJ, Bateman LA, Lin H, Kamenecka T, Lokurkar IA, Lou J, Rao RR, Chang MR, Jedrychowski MP, et al. The secreted enzyme PM20D1 regulates lipidated amino acid uncouplers of mitochondria. Cell. 2016; 166:424–435. [PubMed: 27374330]

Lumeng CN, Saltiel AR. Inflammatory links between obesity and metabolic disease. J Clin Invest. 2011; 121:2111–2117. [PubMed: 21633179]

Lumeng CN, Bodzin JL, Saltiel AR. Obesity induces a phenotypic switch in adipose tissue macrophage polarization. J Clin Invest. 2007; 117:175–184. [PubMed: 17200717]

Madsen KL, Doyle JS, Tavernini MM, Jewell LD, Rennie RP, Fedorak RN. Antibiotic therapy attenuates colitis in interleukin 10 gene-deficient mice. Gastroenterology. 2000; 118:1094–1105. [PubMed: 10833484]

Mauer J, Chaurasia B, Goldau J, Vogt MC, Ruud J, Nguyen KD, Theurich S, Hausen AC, Schmitz J, Brönneke HS, et al. Signaling by IL-6 promotes alternative activation of macrophages to limit endotoxemia and obesity-associated resistance to insulin. Nat Immunol. 2014; 15:423–430. [PubMed: 24681566]

Miller AM, Wang H, Bertola A, Park O, Horiguchi N, Ki SH, Yin S, Lafdil F, Gao B. Inflammation-associated interleukin-6/signal transducer and activator of transcription 3 activation ameliorates alcoholic and nonalcoholic fatty liver diseases in interleukin-10-deficient mice. Hepatology. 2011; 54:846–856. [PubMed: 21725996]

Moldawer LL, Georgieff M, Lundholm K. Interleukin 1, tumour necrosis factor-alpha (cachectin) and the pathogenesis of cancer cachexia. Clin Physiol. 1987; 7:263–274. [PubMed: 3304809]

Moore KW, de Waal Malefyt R, Coffman RL, O'Garra A. Interleukin-10 and the interleukin-10 receptor. Annu Rev Immunol. 2001; 19:683–765. [PubMed: 11244051]

Murray PJ. The primary mechanism of the IL-10-regulated antiinflammatory response is to selectively inhibit transcription. Proc Natl Acad Sci USA. 2005; 102:8686–8691. [PubMed: 15937121]

Murray PJ, Smale ST. Restraint of inflammatory signaling by interdependent strata of negative regulatory pathways. Nat Immunol. 2012; 13:916–924. [PubMed: 22990889]

Nisoli E, Briscini L, Giordano A, Tonello C, Wiesbrock SM, Uysal KT, Cinti S, Carruba MO, Hotamisligil GS. Tumor necrosis factor alpha mediates apoptosis of brown adipocytes and defective brown adipocyte function in obesity. Proc Natl Acad Sci USA. 2000; 97:8033–8038. [PubMed: 10884431]

Odegaard JI, Lee MW, Sogawa Y, Bertholet AM, Locksley RM, Weinberg DE, Kirichok Y, Deo RC, Chawla A. Perinatal licensing of thermogenesis by IL-33 and ST2. Cell. 2016; 166:841–854. [PubMed: 27453471]

Ohno H, Shinoda K, Spiegelman BM, Kajimura S. PPARγagonists induce a white-to-brown fat conversion through stabilization of PRDM16 protein. Cell Metab. 2012; 15:395–404. [PubMed: 22405074]

Parks BW, Nam E, Org E, Kostem E, Norheim F, Hui ST, Pan C, Civelek M, Rau CD, Bennett BJ, et al. Genetic control of obesity and gut microbiota composition in response to high-fat, high-sucrose diet in mice. Cell Metab. 2013; 17:141–152. [PubMed: 23312289]

Parks BW, Sallam T, Mehrabian M, Psychogios N, Hui ST, Norheim F, Castellani LW, Rau CD, Pan C, Phun J, et al. Genetic architecture of insulin resistance in the mouse. Cell Metab. 2015; 21:334–346. [PubMed: 25651185]

Petruzzelli M, Schweiger M, Schreiber R, Campos-Olivas R, Tsoli M, Allen J, Swarbrick M, Rose-John S, Rincon M, Robertson G, et al. A switch from white to brown fat increases energy expenditure in cancer-associated cachexia. Cell Metab. 2014; 20:433–447. [PubMed: 25043816]

Qiu Y, Nguyen KD, Odegaard JI, Cui X, Tian X, Locksley RM, Palmiter RD, Chawla A. Eosinophils and type 2 cytokine signaling in macrophages orchestrate development of functional beige fat. Cell. 2014; 157:1292–1308. [PubMed: 24906148]

Rao RR, Long JZ, White JP, Svensson KJ, Lou J, Lokurkar I, Jedrychowski MP, Ruas JL, Wrann CD, Lo JC, et al. Meteorin-like is a hormone that regulates immune-adipose interactions to increase beige fat thermogenesis. Cell. 2014; 157:1279–1291. [PubMed: 24906147]

Rogers GW, Brand MD, Petrosyan S, Ashok D, Elorza AA, Ferrick DA, Murphy AN. High throughput microplate respiratory measurements using minimal quantities of isolated mitochondria. PLoS ONE. 2011; 6:e21746. [PubMed: 21799747]

Rosen ED, Spiegelman BM. What we talk about when we talk about fat. Cell. 2014; 156:20–44. [PubMed: 24439368]

Sallam T, Jones MC, Gilliland T, Zhang L, Wu X, Eskin A, Sandhu J, Casero D, Vallim TQ, Hong C, et al. Feedback modulation of cholesterol metabolism by the lipid-responsive non-coding RNA LeXis. Nature. 2016; 534:124–128. [PubMed: 27251289]

Saraiva M, O'Garra A. The regulation of IL-10 production by immune cells. Nat Rev Immunol. 2010; 10:170–181. [PubMed: 20154735]

Sartipy P, Loskutoff DJ. Monocyte chemoattractant protein 1 in obesity and insulin resistance. Proc Natl Acad Sci USA. 2003; 100:7265–7270. [PubMed: 12756299]

Seale P, Kajimura S, Yang W, Chin S, Rohas LM, Uldry M, Tavernier G, Langin D, Spiegelman BM. Transcriptional control of brown fat determination by PRDM16. Cell Metab. 2007; 6:38–54. [PubMed: 17618855]

Shoelson SE, Lee J, Goldfine AB. Inflammation and insulin resistance. J Clin Invest. 2006; 116:1793–1801. [PubMed: 16823477]

Siersbæk MS, Loft A, Aagaard MM, Nielsen R, Schmidt SF, Petrovic N, Nedergaard J, Mandrup S. Genome-wide profiling of peroxisome proliferator-activated receptor γin primary epididymal, inguinal, and brown adipocytes reveals depot-selective binding correlated with gene expression. Mol Cell Biol. 2012; 32:3452–3463. [PubMed: 22733994]

Stancáková A, Javorský M, Kuulasmaa T, Haffner SM, Kuusisto J, Laakso M. Changes in insulin sensitivity and insulin release in relation to glycemia and glucose tolerance in 6,414 Finnish men. Diabetes. 2009; 58:1212–1221. [PubMed: 19223598]

Sun L, Goff LA, Trapnell C, Alexander R, Lo KA, Hacisuleyman E, Sauvageau M, Tazon-Vega B, Kelley DR, Hendrickson DG, et al. Long noncoding RNAs regulate adipogenesis. Proc Natl Acad Sci USA. 2013; 110:3387–3392. [PubMed: 23401553]

Tang T, Zhang J, Yin J, Staszkiewicz J, Gawronska-Kozak B, Jung DY, Ko HJ, Ong H, Kim JK, Mynatt R, et al. Uncoupling of inflammation and insulin resistance by NF-kappaB in transgenic mice through elevated energy expenditure. J Biol Chem. 2010; 285:4637–4644. [PubMed: 20018865]

Tiraby C, Langin D. Conversion from white to brown adipocytes: a strategy for the control of fat mass? Trends Endocrinol Metab. 2003; 14:439–441. [PubMed: 14643055]

Tisdale MJ. Biology of cachexia. J Natl Cancer Inst. 1997; 89:1763–1773. [PubMed: 9392617]

Tong AJ, Liu X, Thomas BJ, Lissner MM, Baker MR, Senagolage MD, Allred AL, Barish GD, Smale ST. A stringent systems approach uncovers gene-specific mechanisms regulating inflammation. Cell. 2016; 165:165–179. [PubMed: 26924576]

van Marken Lichtenbelt WD, Vanhommerig JW, Smulders NM, Drossaerts JM, Kemerink GJ, Bouvy ND, Schrauwen P, Teule GJ. Cold-activated brown adipose tissue in healthy men. N Engl J Med. 2009; 360:1500–1508. [PubMed: 19357405]

Villanueva CJ, Waki H, Godio C, Nielsen R, Chou WL, Vargas L, Wroblewski K, Schmedt C, Chao LC, Boyadjian R, et al. TLE3 is a dual-function transcriptional coregulator of adipogenesis. Cell Metab. 2011; 13:413–427. [PubMed: 21459326]

Villanueva CJ, Vergnes L, Wang J, Drew BG, Hong C, Tu Y, Hu Y, Peng X, Xu F, Saez E, et al. Adipose subtype-selective recruitment of TLE3 or Prdm16 by PPARγ specifies lipid storage versus thermogenic gene programs. Cell Metab. 2013; 17:423–435. [PubMed: 23473036]

Virtanen KA, Lidell ME, Orava J, Heglind M, Westergren R, Niemi T, Taittonen M, Laine J, Savisto NJ, Enerbäck S, Nuutila P. Functional brown adipose tissue in healthy adults. N Engl J Med. 2009; 360:1518–1525. [PubMed: 19357407]

Wallenius V, Wallenius K, Ahrén B, Rudling M, Carlsten H, Dickson SL, Ohlsson C, Jansson JO. Interleukin-6-deficient mice develop mature-onset obesity. Nat Med. 2002; 8:75–79. [PubMed: 11786910]

Wernstedt Asterholm I, Tao C, Morley TS, Wang QA, Delgado-Lopez F, Wang ZV, Scherer PE. Adipocyte inflammation is essential for healthy adipose tissue expansion and remodeling. Cell Metab. 2014; 20:103–118. [PubMed: 24930973]

Wu M, Neilson A, Swift AL, Moran R, Tamagnine J, Parslow D, Armistead S, Lemire K, Orrell J, Teich J, et al. Multiparameter metabolic analysis reveals a close link between attenuated mitochondrial bioenergetic function and enhanced glycolysis dependency in human tumor cells. Am J Physiol Cell Physiol. 2007; 292:C125–C136. [PubMed: 16971499]

Wu J, Boström P, Sparks LM, Ye L, Choi JH, Giang AH, Khandekar M, Virtanen KA, Nuutila P, Schaart G, et al. Beige adipocytes are a distinct type of thermogenic fat cell in mouse and human. Cell. 2012; 150:366–376. [PubMed: 22796012]

Xie L, Fu Q, Ortega TM, Zhou L, Rasmussen D, O'Keefe J, Zhang KK, Chapes SK. Overexpression of IL-10 in C2D macrophages promotes a macrophage phenotypic switch in adipose tissue environments. PLoS ONE. 2014; 9:e86541. [PubMed: 24466141]

Zambelli F, Pesole G, Pavesi G. Pscan: finding over-represented transcription factor binding site motifs in sequences from co-regulated or co-expressed genes. Nucleic Acids Res. 2009; 37:W247–W252. [PubMed: 19487240]

Highlights

- Mice lacking IL-10 have increased energy expenditure and adipose thermogenesis

- IL-10 acts on IL-10Rα in adipose tissue to antagonize adrenergic tone

- IL-10Rα knockdown promotes the browning of subcutaneous white adipose tissue

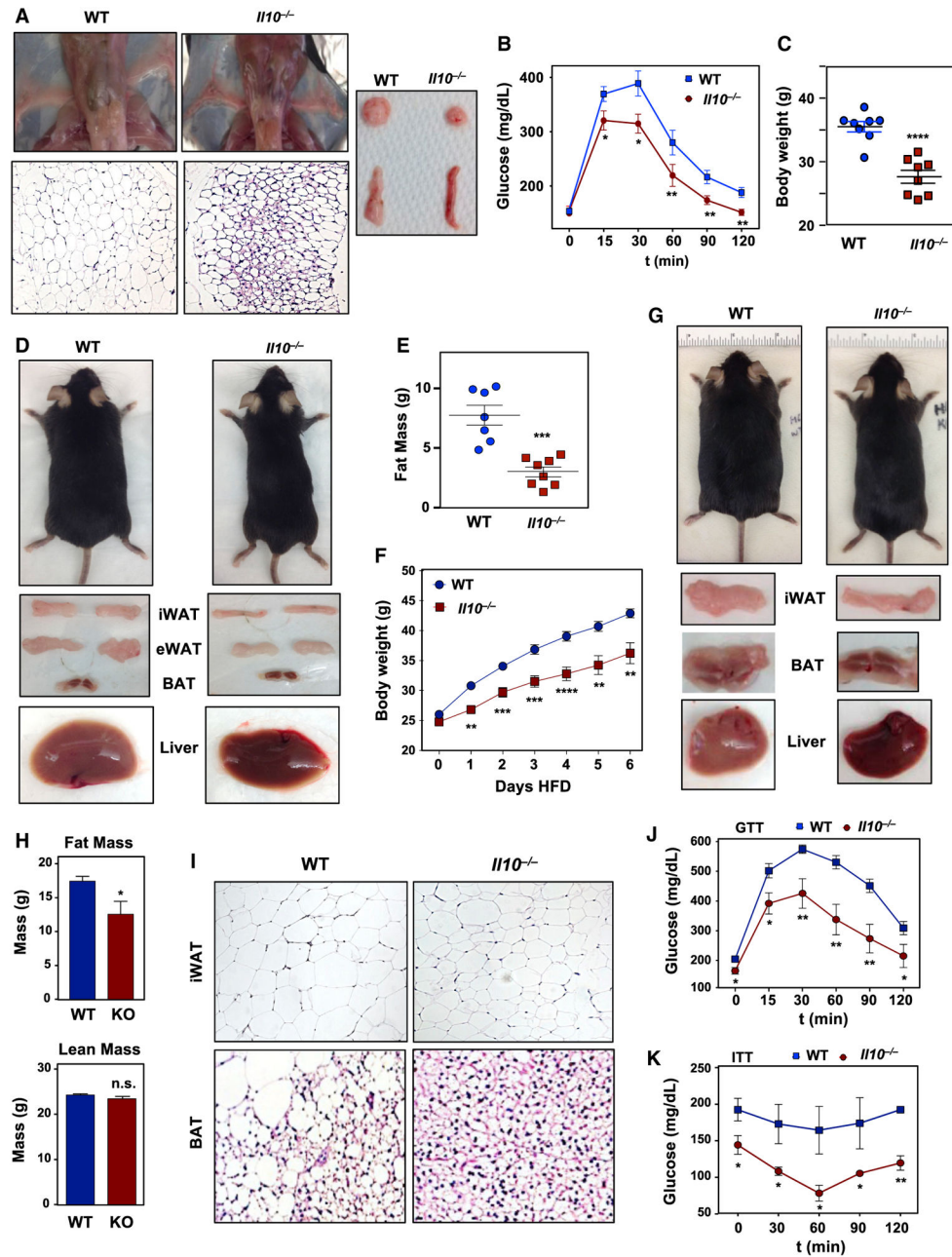- IL-10 affects chromatin structure and C/EBPβ and ATF occupancy at thermogenic genes

Figure 1. IL-10-Deficient Mice Are Protected against Obesity

(A) Representative images of 10-week-old chow-fed WT and *Il-10*−/− mice showing gross adipose tissue appearance and histology (H&E).

(B) Intraperitoneal (i.p.) glucose tolerance test performed on 10-week-old chow-fed mice. N = 7. Comparisons at each time point were made against WT control mice by repeated measures ANOVA.

(C) Body weight of 32-week-old chow-fed WT and *Il-10*−/− mice. N = 8, 4.

(D) Gross appearance of representative 32-week-old chow-fed mice and their tissue.

(E) Body fat mass of 32-week-old chow-fed mice determined by EchoMRI. N = 8.

(F) Body weight of mice fed chow diet for 10 weeks and then on a 60% high-fat diet (HFD) for 6 weeks. N = 16, 12. Statistical analysis was performed using Student's t test.

(G) External and gross tissue appearance of representative 6-week-old mice that were HFD-fed.

(H) Fat and lean mass of mice in (F). Statistical analysis was performed using Student's t test.

(I) Representative histology of iWAT and BAT from mice in (F).

(J) An i.p. glucose tolerance test (GTT) was performed on WT and *Il-10$^{-/-}$* mice fed chow diet for 10 weeks and then on a 60% HFD for 6 weeks. N = 7.

(K) An i.p. insulin tolerance test (ITT) was performed on mice in (J). N = 7. Comparisons at each time point were made against WT control mice by repeated measures ANOVA. *p < 0.05, **p < 0.01, ***p < 0.001, ****p < 0.0001, ns, not significant.

Error bars represent SEM. See also Figure S1.
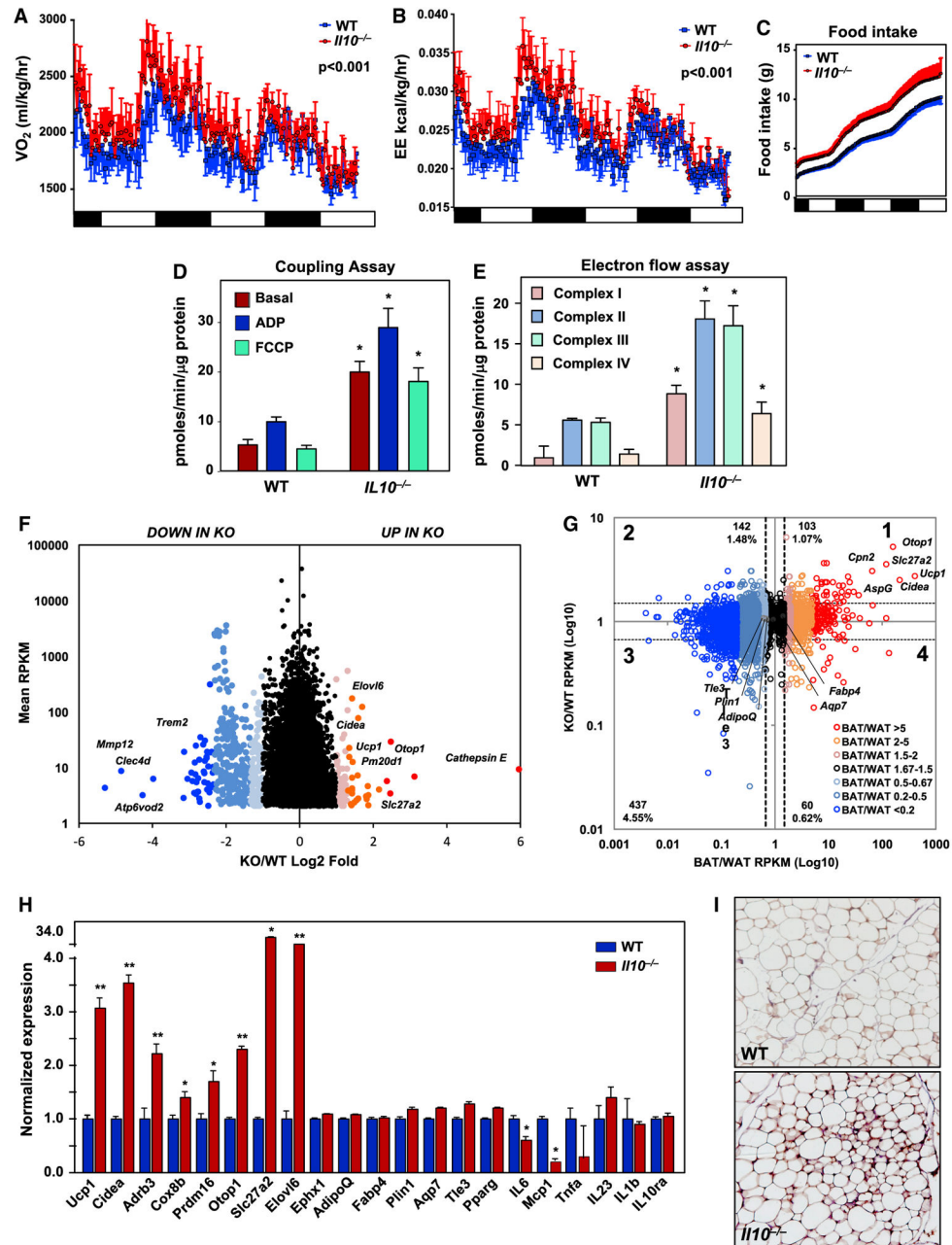
Figure 2. IL-10 Deficiency Promotes Energy Expenditure and Adipose Tissue Browning

(A–C) Energy expenditure (EE) (kCal/kg/hr) (A), VO₂ (mL/kg/hr) (B), and food intake (g)
(C) of chow-fed 10-week-old WT and *Il-10⁻/⁻* mice was analyzed by Columbus Oxymax
metabolic chambers. 12-hr light/dark cycles; 72-hr total duration; and each light/dark bar
represents 12 hr duration. N = 7. Statistical analysis was performed using two-way ANOVA
and ANCOVA.

(D and E) Average oxygen consumption rate (OCR) of mitochondria isolated from iWAT in
mitochondrial coupling (D) and electron flow assays (E). Samples were treated with
different substrates or inhibitors to obtain specific respiration states as indicated. Data are

the average of six internal replicates and are representative of two experiments. Statistical analysis was performed using Student's t test.

(F) Scatterplot of gene expression differences between WT and *Il-10^−/−* mice as determined by RNA sequencing of iWAT. Genes with at least 4 RPKM are shown. The log2 ratio of KO/WT expression (x axis) is shown as a function of max RPKM (y axis), with select genes indicated with vertical text. Shades of blue correspond to genes downregulated in the *Il-10^−/−* mice, and shades of red indicate upregulation in *Il-10^−/−* mice. N = 9, 11.

(G) Scatterplot of the gene expression ratio in *Il-10^−/−* to WT mice versus BAT to WAT (Seale et al., 2007). Genes are color-coded based on the expression ratio of BAT to WAT, and the dash lines represent the cutting range of the gene expression ratio, 0.67 and 1.5 accordingly. Genes that are strongly upregulated in *Il-10^−/−* mice are enriched in BAT-selective genes (red annotated genes). WAT-selective genes (black annotated genes) with similar expression in *Il-10^−/−*, and WT mice were either weakly repressed or similar in BAT.

(H) Real-time analysis of gene expression in iWAT from WT and *Il-10^−/−* mice. N = 9, 11.

(I) Immunohistochemical staining for UCP1 in iWAT. $*p < 0.05$, $**p < 0.01$.

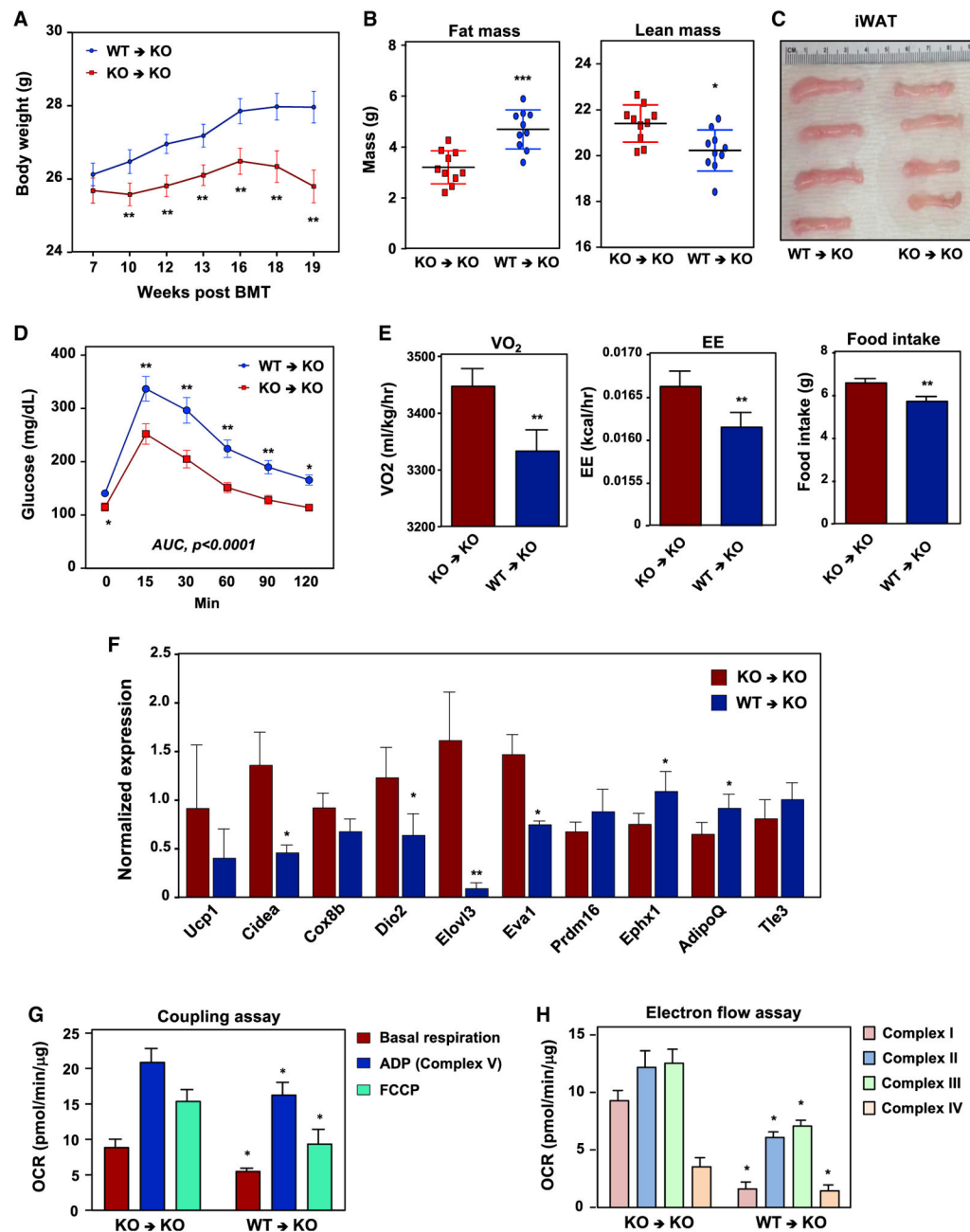Error bars represent SEM. See also Figure S2.

Figure 3. Bone-Marrow-Derived IL-10 Inhibits Thermogenesis

(A) Body weight of lethally irradiated chow-fed *Il-10*^{−/−} mice reconstituted with WT (WT→KO) or *Il-10*^{−/−} (KO→KO) bone marrow 7 weeks post-transplant. N = 10. Statistical analysis was performed using Student's t test.

(B) Body fat and lean mass of WT→KO and KO→KO mice determined by EchoMRI.

(C) Gross appearance of iWAT 19 weeks post-BMT.

(D) An i.p. GTT was performed on WT→KO and KO→KO mice. N = 10. Comparisons at each time point were made by repeated measures ANOVA.

(E) EE, VO$_2$, and food intake were analyzed by metabolic chambers. 12-hr light/dark cycles; 72-hr total duration; and each light/dark bar represents 12-hr duration. N = 10 per group. Statistical analysis was performed using two-way ANOVA and ANCOVA.

(F) Gene expression in iWAT determined by real-time PCR. N = 9. Statistical analysis was performed using Student's t test.

(G and H) Average oxygen consumption rate (OCR) in coupling (G) and electron flow (H) assays of mitochondria isolated from iWAT of WT→KO and KO→KO mice. Data are the average of six internal replicates and are representative of two experiments. Statistical analysis was by Student's t test. *p < 0.05, **p < 0.01, ***p < 0.001.

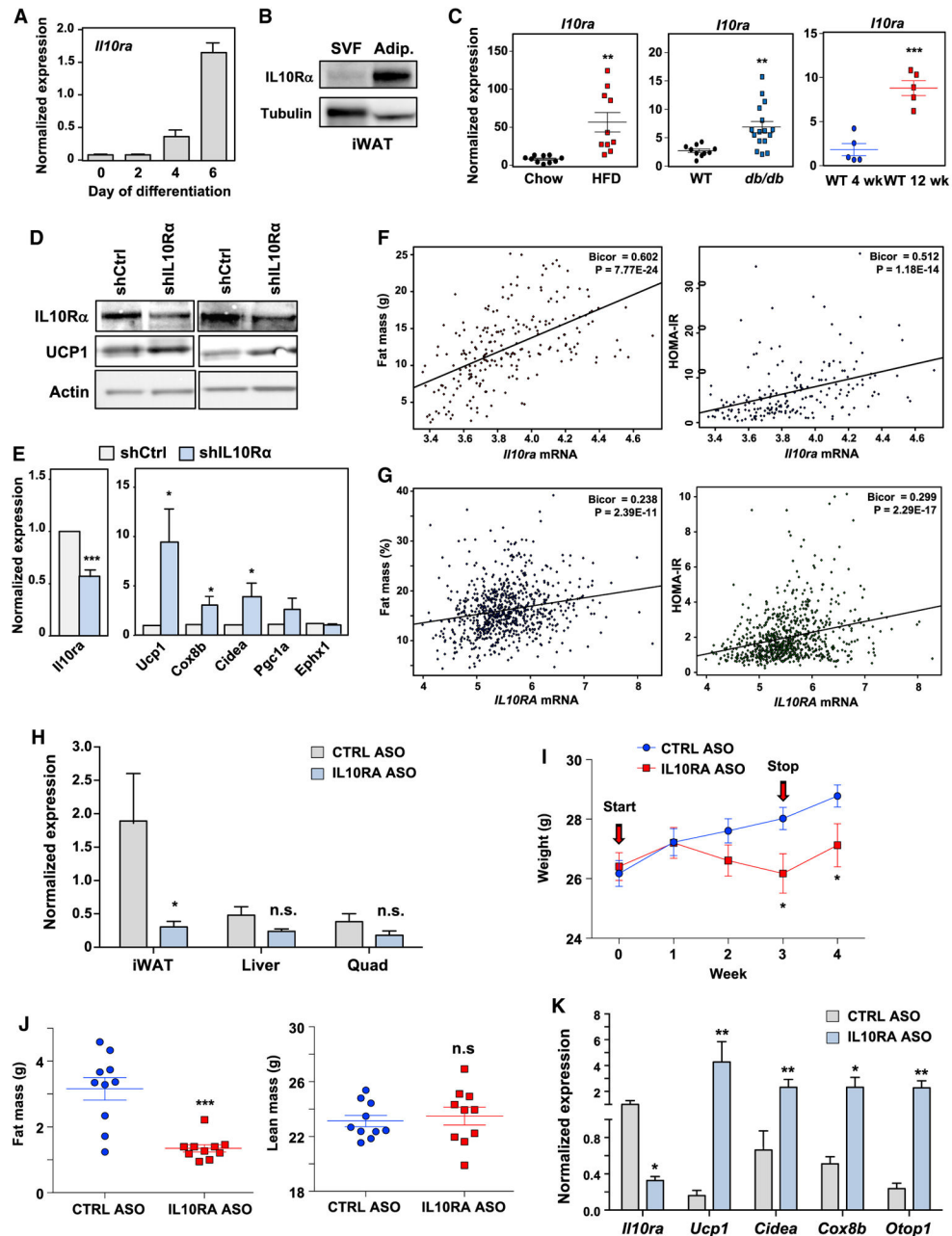Error bars represent SEM. See also Figure S3.

Figure 4. Adipose IL-10Rα Knockdown Increases Thermogenenic Gene Expression

(A) Real-time PCR analysis of *Il-10ra* mRNA during the differentiation of primary iWAT stromal vascular fraction (SVF). Cells were stimulated to differentiate with dexamethasone (1 μM), IBMX (0.5 mM), insulin (5 μg/mL), and rosiglitazone (20 nM) for 2 days, followed by insulin and rosiglitazone for 5 days.

(B) Immunoblot analysis of IL-10Rα expression in SVF and adipocyte fraction of iWAT from chow-fed 10-week-old mice.

(C) *Il-10ra* mRNA from iWAT of 12-week-old chow or HFD-fed mice, 12-week-old WT or *db/db* mice, and 4- and 12-week-old chow-fed WT mice. Statistical analysis was performed using Student's t test. **N** = 5–15.

(D) Immunoblot analysis of protein from iWAT of 10-week-old mice injected with 2×10^9 plaque-forming units (PFUs) of the adenovirus-expressing control shRNA (shCtrl) or the shRNA targeting IL-10Rα for 72 hr. Each lane represents an individual animal.

(E) Gene expression in iWAT transduced with shCtrl or shIL-10Rα adenovirus. Data represent the average of 8–10 mice/group. Statistical analysis was performed using Student's t test.

(F and G) Correlation trait plots of IL-10Rα expression and fat mass and HOMA-IR data from the HMDP (F) and the METSIM (G) studies. All correlations were assessed from the midweight bicorrelation coefficient and corrected p value using the R package WGCNA (Langfelder and Horvath, 2008).

(H) *Il-10ra* expression in tissues from ctrl or IL-10Rα ASO-treated mice.

(I) Body weight of 12-week-old mice treated with ctrl or IL-10Rα ASO for 3 weeks.

(J) Fat mass and lean mass of mice in (I).

(K) Gene expression in iWAT from mice treated with ctrl or IL-10Rα ASO. N = 10 per group. *p < 0.05, **p < 0.01, ***p < 0.001, ****p < 0.0001, ns, not significant. Error bars represent SEM. See also Figure S4.
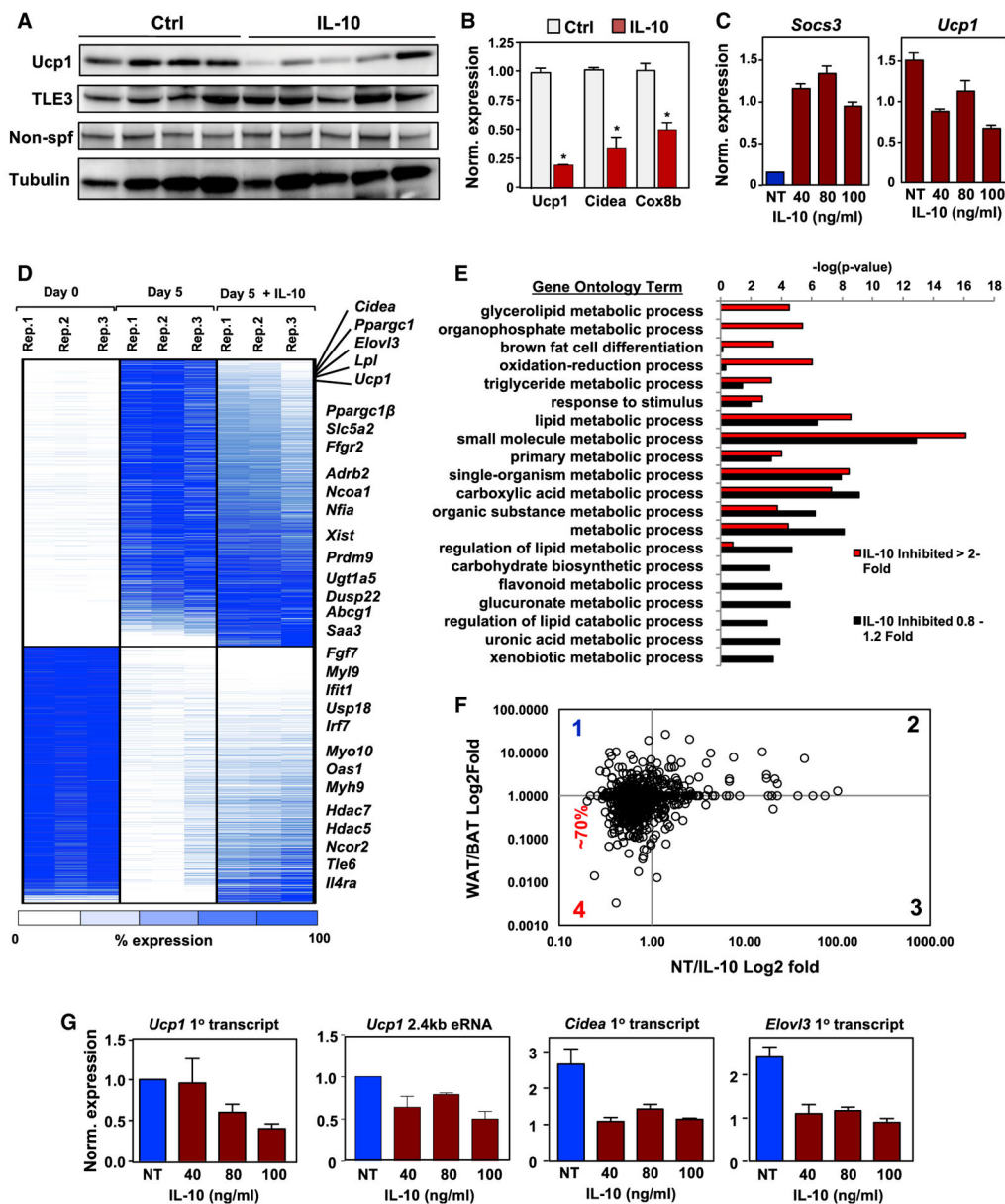
Figure 5. IL-10 Directly Acts on Adipocyte IL-10Rα to Inhibit Thermogenesis

(A) Immunoblot analysis of protein extracts from iWAT of 10-week-old mice treated *ex vivo* with vehicle (ctrl) or 100 ng/mL IL-10. N = 4–6. Results are representative of three independent experiments.

(B) Real-time PCR analysis of gene expression in iWAT of 10-week-old mice treated *ex vivo* with control (NT) or 100 ng/mL IL-10 for 1 hr. N = 4–6.

(C) Gene expression in brown differentiated iBAd cells treated with recombinant IL-10 for 16 hr.

(D) Heatmap representation of genes that changed >3-fold (p < 0.01) by RNA-seq on day 5 (D5) of differentiation of iBAd cells. Each sample is shown in triplicate and compared to expression at day 0 (D0). Genes are grouped as either induced upon differentiation (top) or

repressed during differentiation (bottom). The far-right column shows the effect of 100 ng/mL IL-10 treatment on gene expression at D5. Genes are ranked based on IL-10 inhibition, with selected genes shown in the text at right.

(E) Genes induced upon differentiation were divided based on their response to IL-10, either inhibited >2-fold (red bars) or not affected (black bars), and gene ontology analysis was performed with –log10 (p value) plotted (x axis) as a function of classification meeting a p value of < 0.001.

(F) RNA-seq data from the *in-vitro*-differentiated WAT/BAT ratio (Sun et al., 2013) plotted as a function of RNA-seq data from the NT/IL-10 ratio.

(G) Real-time PCR analysis of primary mRNA transcripts and *Ucp1* eRNA in iBAd cells on D5 with and without IL-10 for 16 hr. $*p < 0.05$, $**p < 0.01$, $***p < 0.001$, $****p < 0.0001$, ns, not significant.

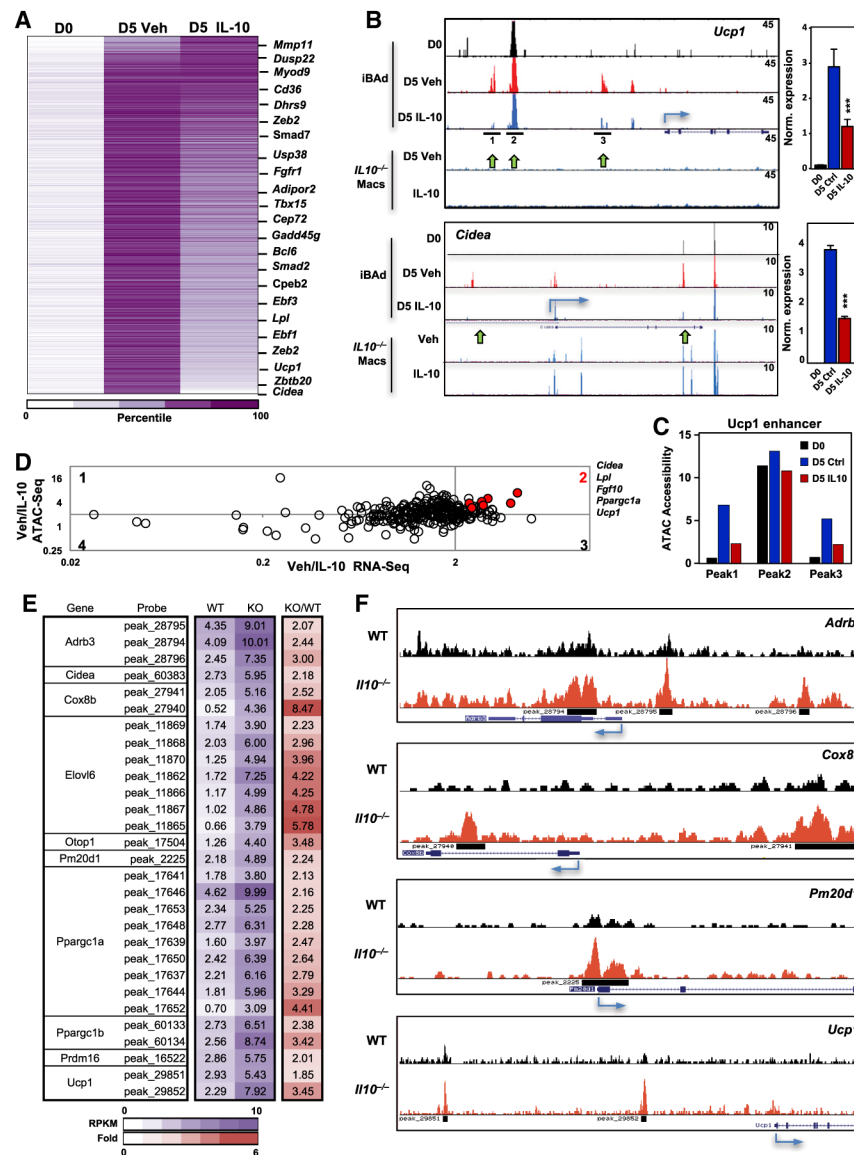Error bars represent SEM. See also Figure S5.

Figure 6. IL-10 Signaling Remodels Chromatin Architecture at Thermogenic Genes

(A) Heatmap analysis of ATAC-seq performed on D0 and D5 of iBAd cell differentiation with and without 100 ng/mL IL-10 for 16 hr for all called peaks demonstrating >5-fold induction (N = 3,174 sites). Peaks were assigned to the nearest gene, and the selected genes are shown.

(B) ATAC-seq bedgraph panels of the *Ucp1* and *Cidea* loci showing peak locations relative to the transcription start site (TSS). Panels compare ATAC signals between iBAd cells to signals from *Il-10*−/− bone-marrow-derived macrophages (macs) treated with and without 30 ng/mL IL-10. Adjacent to the ATAC panel is real-time PCR analysis of gene expression.

(C) ATAC peak strength (y axis) for selected peaks within the *Ucp1* locus under the indicated conditions.

(D) Correlation plot of ATAC-seq and RNA-seq data.

(E) Merged heatmap analysis of ATAC-seq performed on adipocytes derived from 10-week-old mice showing enhanced chromatin accessibility in *Il-10*$^{-/-}$ mice at peaks annotated to BAT-selective genes. N = 2.

(F) ATAC-seq bedgraph panels of the indicated gene loci showing peak locations relative to the TSS. *p < 0.05, **p < 0.01, ***p < 0.001.

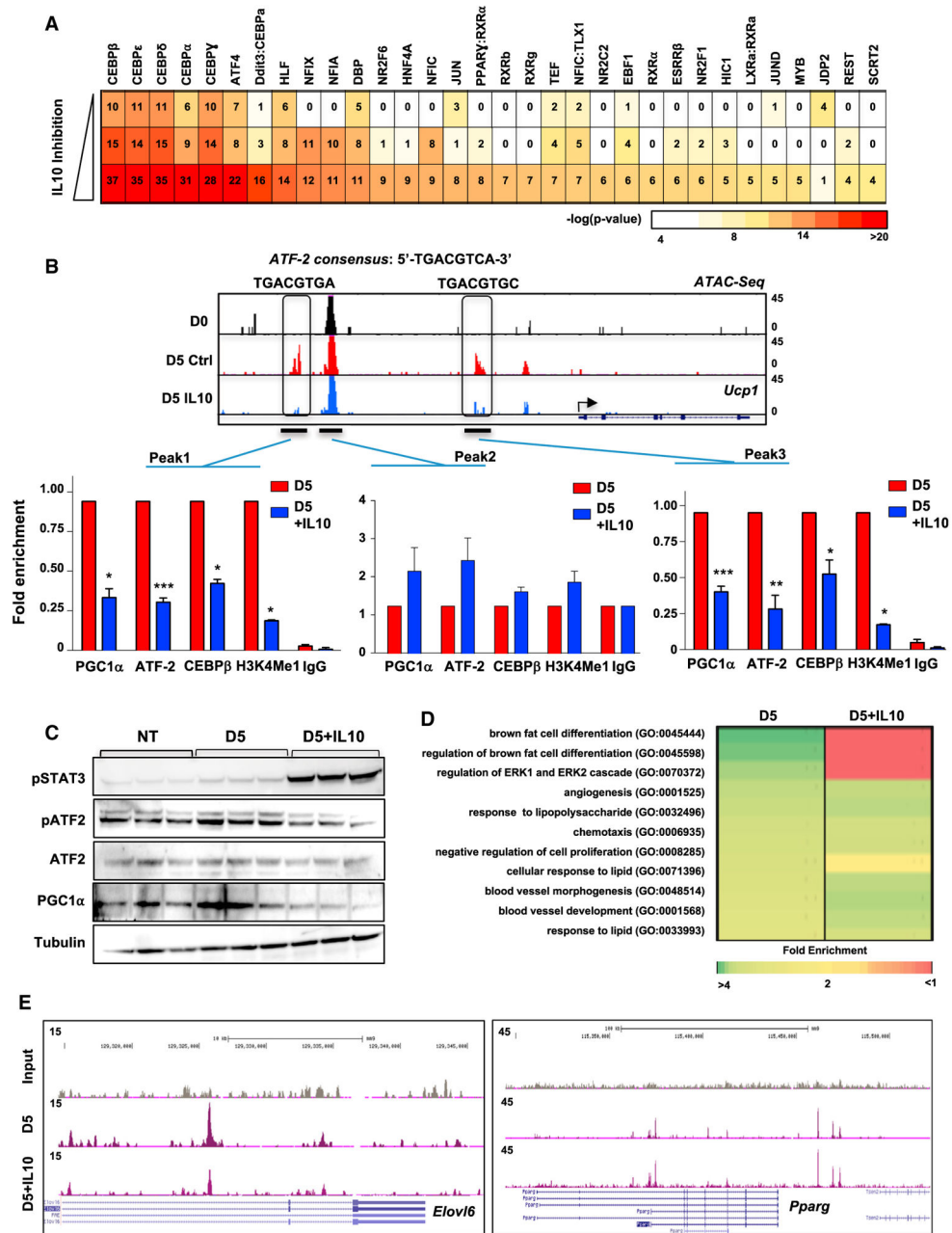Error bars represent SEM. See also Figure S6.

Figure 7. IL-10 Limits the Recruitment of Thermogenic Transcriptional Regulators

(A) TF motif analysis of ten bins containing 3,174 ATAC peaks demonstrating the highest fold induction during maturation separated into three groups of 1,058 peaks based on the degree of IL-10 inhibition.

(B) ChIP-qPCR was performed for indicated proteins on iBAd cells treated with and without 100 ng/mL IL-10 for 16 hr.

(C) Immunoblot analysis of proteins from differentiated iBAd cells treated with and without IL-10 for 16 hr.